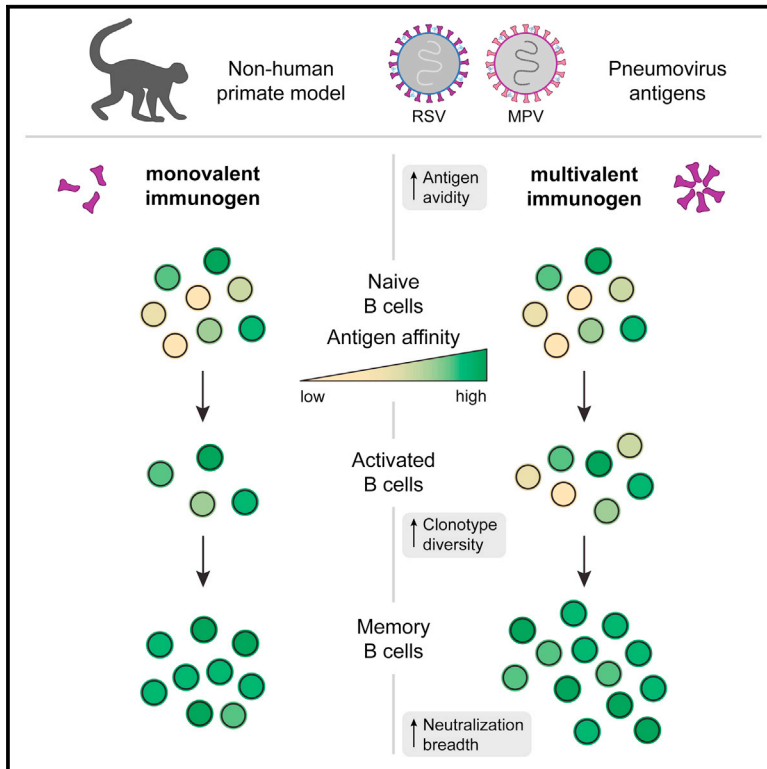# Immunity

Multivalent antigen display on nanoparticle immunogens increases B cell clonotype diversity and neutralization breadth to pneumoviruses

Graphical abstract

Authors

Sebastian Ols, Klara Lenart, Rodrigo Arcoverde Cerveira, ..., Tracy J. Ruckwardt, Neil P. King, Karin Loré

Correspondence

karin.lore@ki.se

In brief

A mechanistic understanding of immune responses elicited by multivalent nanoparticle immunogens is lacking in higher mammals. Ols et al. show in non-human primates that humoral responses are modulated by interrelated aspects of nanoparticles: their size and valency. Nanoparticle size slowed lymphatic transport, and valency-dependent avidity improved recruitment of low-affinity B cells, increasing B cell clonotype diversity and neutralization breadth.

Highlights

- Increased immunogen size slows kinetics of antigen accumulation in lymph nodes

- High antigen valency restricts access to base-proximal epitopes on displayed antigens

- Avidity effects from higher valency drive recruitment of more diverse B cell clonotypes

- Antibodies with high potency or breadth can affinity mature from low-affinity precursors

CellPress

Article

Multivalent antigen display on nanoparticle immunogens increases B cell clonotype diversity and neutralization breadth to pneumoviruses

Sebastian Ols,[1,2] Klara Lenart,[1,2,9] Rodrigo Arcoverde Cerveira,[1,2,9] Marcos C. Miranda,[1,2] Natalie Brunette,[3,4] Jana Kochmann,[1,2] Martin Corcoran,[5] Rebecca Skotheim,[3,4] Annika Philomin,[3,4] Alberto Cagigi,[1,2] Brooke Fiala,[3,4] Samuel Wrenn,[3,4] Jessica Marcandalli,[6] Fredrika Hellgren,[1,2] Elizabeth A. Thompson,[1,2] Ang Lin,[1,2] Florian Gegenfurtner,[1,2] Azad Kumar,[7] Man Chen,[7] Ganesh E. Phad,[5,6] Barney S. Graham,[7] Laurent Perez,[8] Andrew J. Borst,[3,4] Gunilla B. Karlsson Hedestam,[5] Tracy J. Ruckwardt,[7] Neil P. King,[3,4,10] and Karin Loré[1,2,10,11,*]

[1]Division of Immunology & Allergy, Department of Medicine Solna, Karolinska Institutet, and Karolinska University Hospital, Stockholm, Sweden
[2]Center for Molecular Medicine, Karolinska Institutet, Stockholm, Sweden
[3]Department of Biochemistry, University of Washington, Seattle, WA, USA
[4]Institute for Protein Design, University of Washington, Seattle, WA, USA
[5]Department of Microbiology, Tumor and Cell Biology, Karolinska Institutet, Stockholm, Sweden
[6]Università della Svizzera italiana, Faculty of Biomedical Sciences, Institute for Research in Biomedicine, Bellinzona, Switzerland
[7]Vaccine Research Center, National Institute of Allergy and Infectious Diseases, National Institutes of Health, Bethesda, MD, USA
[8]University of Lausanne (UNIL), Lausanne University Hospital (CHUV), Department of Medicine, Service of Immunology and Allergy, and Center for Human Immunology (CHIL), Lausanne, Switzerland
[9]These authors contributed equally
[10]Senior author
[11]Lead contact
*Correspondence: karin.lore@ki.se
https://doi.org/10.1016/j.immuni.2023.08.011

SUMMARY

Nanoparticles for multivalent display and delivery of vaccine antigens have emerged as a promising avenue for enhancing B cell responses to protein subunit vaccines. Here, we evaluated B cell responses in rhesus macaques immunized with prefusion-stabilized respiratory syncytial virus (RSV) F glycoprotein trimer compared with nanoparticles displaying 10 or 20 copies of the same antigen. We show that multivalent display skews antibody specificities and drives epitope-focusing of responding B cells. Antibody cloning and repertoire sequencing revealed that focusing was driven by the expansion of clonally distinct B cells through recruitment of diverse precursors. We identified two antibody lineages that developed either ultra-potent neutralization or pneumovirus cross-neutralization from precursor B cells with low initial affinity for the RSV-F immunogen. This suggests that increased avidity by multivalent display facilitates the activation and recruitment of these cells. Diversification of the B cell response by multivalent nanoparticle immunogens has broad implications for vaccine design.

INTRODUCTION

Antibody responses that can neutralize or help clear pathogens are the primary correlate of protection for licensed human vaccines.[1] The quality and durability of elicited antibody responses vary widely between vaccines, for reasons that are not fully understood. A better understanding of the interactions between B cells and their cognate antigen is necessary for rational vaccine design. Non-live protein subunit vaccines remain a cornerstone of modern vaccine design but are poorly immunogenic without co-formulation with adjuvants or formulation in or on nanoparticles for display.[2] Multivalent antigen display is strongly associated with higher antibody titers and therefore likely has a direct influence on the interaction with B cells. Yet, mechanistic studies *in vivo* of how antigen valency affects the B cell response are very limited.

Upon encounter of cognate antigens, B cells are activated and instructed through the germinal center (GC) reaction to undergo affinity maturation in order to fine-tune the specificity of their B cell receptors (BCRs).[3] Further specialization through somatic hypermutation (SHM) ultimately generates an antibody response of high affinity. The initial selection of B cells is dependent on the reactivity of the immunoglobulin (Ig) variable, diversity, and joining (VDJ) gene recombination they carry and the affinity this imparts for their cognate antigen. The role of multivalent particulate antigens in shaping the selection and diversification of
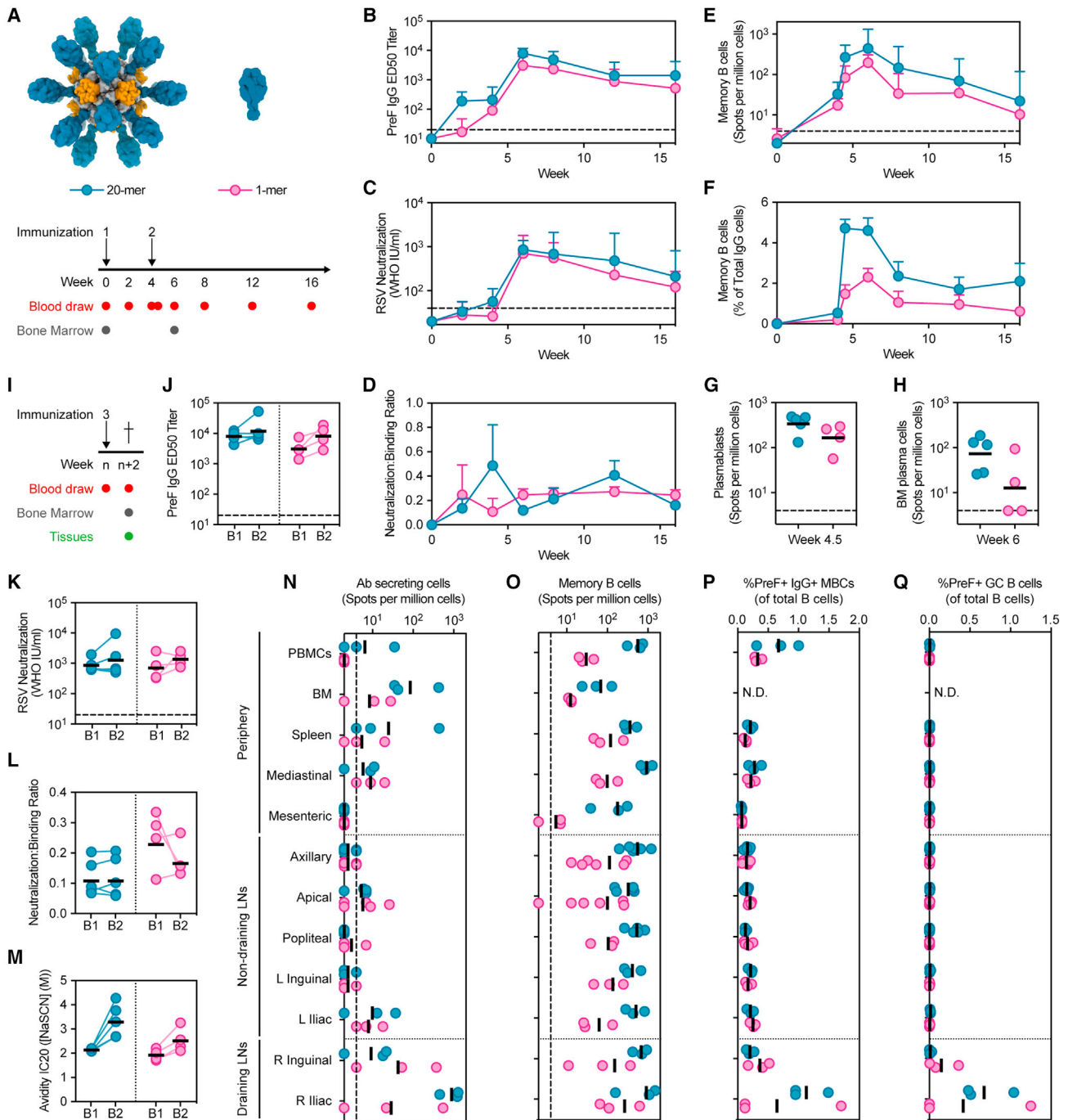
Figure 1. Multivalent display enhances the magnitude of B cell responses

(A–H) Naive rhesus macaques were immunized in the right quad by intramuscular injection at weeks 0 and 4 with 20-mer or 1-mer preF (DS-Cav1) immunogens in SWE adjuvant as depicted in (A).

(B–D) Plasma preF-binding IgG titers (B), RSV neutralization titers (C), and the neutralization to binding ratio (D) measured over the course of 16 weeks.

(E and F) PreF-specific memory B cells in peripheral blood mononuclear cells (PBMCs) assessed by ELISpot over the course of 16 weeks. Plotted as number of preF-specific cells (E) or as a percentage of IgG-secreting cells (F).

(G) PreF-specific plasmablasts in PBMCs measured by ELISpot 4 days after boost 1 (week 4.5).

(H) PreF-specific plasma cells in bone marrow (BM) measured by ELISpot at week 6.

(I–Q) Rhesus macaques received a third immunization (boost 2 [B2]) of their respective immunogen at week 18 (n = 3 per group) or week 36 (n = 2 for 20-mer and n = 1 for 1-mer). 2 weeks after the third immunization (week 20), animals were euthanized, and tissues were harvested.

(J) PreF-binding IgG titers of plasma measured at week 6 (boost 1 [B1]) and 2 weeks after boost 2 (B2).

(K and L) RSV neutralization of plasma (K) and the neutralization to binding ratio (L) measured at the same time points as in (J).

the B cell response is not fully understood. We have earlier demonstrated that multivalent display enhances antibody responses in a valency-dependent manner,[4] indicating that avidity may play a role as well as increased BCR cross-linking. Improved transport of multivalent antigens to the B cell follicles in lymph nodes (LNs) through increased immunogen size and complement activation has also been reported.[5–10] Understanding these immunological functions and how they can be better harnessed to fine-tune immune responses to protein antigens is critical for improved vaccine design. Recently, an elegant study used a wide range of antigen valencies on several distinct nanoparticle scaffolds of varying sizes to study the *in vivo* effects on transgenic B cells in an adoptive transfer mouse model.[11] Antigen valency was shown to dictate the composition of the transgenic B cell response and enhance the recruitment of lower-affinity, non-transgenic endogenous B cells. Expanding on such findings in outbred higher-order mammals is required to further our understanding of B cell responses and vaccine design.

Multiple strategies for multivalent antigen display exist,[12] with synthetic nanoparticles, such as liposomes, and naturally occurring self-assembling protein scaffolds, such as lumazine synthase and ferritin, being commonly used as platforms to present a variety of protein antigens.[13–16] Self-assembling proteins are a clinically validated vaccine modality with an established record of safety and efficacy, and the multivalent nature of the virus-like particle used for licensed human papillomavirus vaccines is considered crucial for its potent immunogenicity.[12] Recently, computationally designed hyperstable protein nanoparticles have been adapted for presentation of protein antigens from a multitude of pathogens.[4,17–21] The ability to precisely modulate several features of designed nanoparticle immunogens, including the valency, geometry, and identity of the displayed antigens, makes them attractive tools for studying the effects of multivalent display *in vivo*.

Furthermore, advancements in structure-based antigen design have improved the elicitation of potent humoral immune responses to non-live protein subunit vaccines. This process uses atomic-level information to identify and stabilize neutralization-sensitive epitopes of viral protein antigens.[22] The subunit vaccine candidate based on the prefusion (preF)-stabilized respiratory syncytial virus (RSV) fusion (F) glycoprotein (DS-Cav1) has been at the forefront of structure-guided vaccine design efforts and has shown promise in mice and macaques,[23] as well as in humans.[24–26] The preF conformation of the RSV-F protein exposes more neutralization-sensitive epitopes than the postfusion (postF) conformation and accounts for most of the neutralizing activity of the infection-induced antibody response in humans.[27,28]

In this study, we utilized the rhesus macaque model to characterize the immune response elicited by immunization with nanoparticles displaying either 10 or 20 copies of RSV preF (DS-Cav1) trimer[4] and compared these with single trimer subunit (1-mer) preF or postF immunization. We studied the abilities of the nanoparticle, both as a vehicle for the transport of antigen and a scaffold for multivalent display, to define their effects on the B cell response. Importantly, we show that multivalent display can overcome suboptimal epitope targeting through avidity effects that broaden the diversity of responding B cells to also include cross-reactive B cells recognizing a related pneumovirus. These findings have important implications for future vaccine design, highlighting critical features of multivalent display and its effects on primate B cell responses.

RESULTS

Multivalent display enhances the magnitude of B cell responses

We have previously shown that multivalent display of preF as a 20-mer nanoparticle elicits potent humoral immune responses in mice and rhesus macaques.[4] Here, we addressed the mechanistic basis of this potency by performing detailed analyses of nanoparticle vaccine trafficking and defining antibody epitope specificities and the clonality of vaccine-induced memory B cells (MBCs). Prime-boost immunization of rhesus macaques at weeks 0 and 4 with 20-mer or single "soluble" trimer (1-mer) preF immunogens in the oil-in-water adjuvant squalene oil-in-water emulsion (SWE) elicited robust circulating antibody responses (Figures 1A and 1B), whereas 20-mer immunization without adjuvant elicited substantially reduced responses in comparison (Figures S1A–S1C). The primary immunogenicity endpoint of neutralizing antibody activity followed a similar dynamic to binding antibody responses (Figure 1C) and resulted in similar antibody quality as assessed by the neutralization to binding ratio metric (Figure 1D). Increased output of antigen-specific MBCs and plasmablasts in peripheral blood as well as plasma cells in bone marrow (BM) was observed with 20-mer immunization as assessed by ELISpot (Figures 1E–1H). T cell responses, assessed by a peptide recall assay, were detectable at comparable levels with both immunogens (Figure S1D). Hence, in the presence of an adjuvant, two doses of the 20-mer-induced robust B cell responses at equivalent or higher levels to the 1-mer immunogen.

The administration of a third dose at week 18 or 36 (boost 2 [B2]) normalized antibody quantity and quality between the 20-mer and 1-mer immunogens (Figures 1I–1M). Memory B and T cell responses were detected in multiple lymphoid and non-lymphoid tissues, with overall higher cell numbers and

---

(M) PreF-specific IgG avidity as measured by a chaotropic wash ELISA with sodium thiocyanate (NaSCN). Molar concentration of NaSCN needed to dissociate 20% of binding (IC20) is plotted at the same time points as in (J).

(N–Q) Quantification of PreF-specific B cells in different tissues at week 20 (2 weeks after boost 2; n = 3 per group) by ELISpot (N and O) or flow cytometry (P and Q) Memory B cells (MBCs) were defined as CD20+ IgG+ BCL6− cells (P) and germinal center (GC) B cells as CD20+ BCL6+ Ki67+ cells (Q). N.D., not determined/analyzed.

(B, C, and E) Data points represent geometric mean, and error bars are geometric SD. (D and F) Data points represent arithmetic mean, and error bars are SEM. (G–O) Bars depict geometric mean. (G–M) Data points represent individual animals (n = 4–5 per group). (P and Q) Bars depict arithmetic mean. (N–Q) Data points represent individual tissue samples (n = 3–6 per group). Statistical significance was assessed by two-tailed Mann-Whitney U test with a false discovery rate correction for multiple comparisons.

See also Figure S1.

frequencies induced by 20-mer immunization (Figures 1N–1Q, S1E, and S1F). Consistent with other studies, antigen-specific GC B cells were only detected in the vaccine-draining LNs (Figure 1Q), indicating restricted localization of priming of adaptive immune responses.[29,30] Together, these data suggest that the 20-mer may possess an advantage in activating B cells because of its increased size, the dense and repetitive presentation of antigen on the nanoparticle surface, or both.

Larger size of multivalent nanoparticles delays kinetics of LN accumulation

Immunogen size can directly modulate immune cell and tissue targeting as well as the kinetics of lymphatic drainage, with downstream effects on vaccine-elicited antibody responses.[5,6] We investigated differences in vaccine dissemination by utilizing Alexa Fluor 647-labeled 16-mer nanoparticles or 1-mer immunogens (Figure 2A). This allowed us to longitudinally examine the interactions with immune cells in single-cell suspensions of the intramuscular (I.M.) injection site and vaccine-draining LNs at 2 h and 1, 3, and 7 days post-immunization (Figures 2B, 2G, and S2A). Both immunogens induced robust vaccine uptake and targeted similar immune cell subsets at the site of injection and in the draining LNs at all time points analyzed (Figures 2B–2K and S2C–S2H). The increased frequency of vaccine-positive cells in the muscle observed 2 h post-immunization with the 1-mer (Figures 2B–2E) may in part be explained by the 16-fold lower molarity of the nanoparticle, which derived from administering equimolar antigen doses (i.e., preF). This dose-dependent effect was clear *in vitro* when using varying molarities (Figure S2B). *In vivo*, the largest difference was in the kinetics of antigen accumulation in LNs (Figures 2G–2L). Although both immunogens targeted the same LNs draining the muscle (Figures S2C and S2D), the 1-mer rapidly accumulated in LNs, reached a peak at 2 h post-administration and rapidly dissipated from its peak, whereas the nanoparticle gradually reached a peak around day three (Figures 2H–2L, S2E, and S2F). These data suggest that the larger size of multivalent immunogens may restrict their transport *in vivo*, effectively slowing the kinetics of their accumulation in LNs, and could be a significant contributor to enhanced antigen retention[31,32] and improved immunogenicity, reminiscent of the effects of slow-release immunization strategies.[33,34] Mannose-binding lectin (MBL) was not implicated in the immunogen trafficking observed in this study (Figure S2I) because of the lack of mannosylation on RSV-F,[35] although it may play an important role in the trafficking of other multimerized antigens.[7,10] Thus, immunogen size may independently modulate immunogenicity in primates.

Valency-dependent skewing of serum antibody specificities

Next, we hypothesized that preferential exposure of antigenic epitopes on the nanoparticle immunogen could influence B cell selection and the epitope specificities of vaccine-elicited antibodies.[17,18] Roughly, 60% of the antigenic surface is shared between the preF and postF conformations (hereafter referred to as the "preF/postF shared surface area"), and these surfaces primarily make up the equatorial region of the preF conformation and the apex of the postF conformation (Figure 3A).[36,37] Both serum-neutralizing activity and preF binding were substantially

reduced by depleting postF- and preF/postF-shared surface area-specific antibodies using postF protein (Figures 3A–3C, S3A, and S3B). The reactivity to the preF/postF-shared surface area trended higher in the 20-mer animals, suggesting skewing of the antibody response. Neither immunogen elicited a high proportion of solely postF-specific antibodies (Figures 3D and S3C).

To test if the specificity skewing was an intrinsic feature of 20-mer immunization, we boosted a new set of macaques that had earlier been primed with 1-mer preF immunogens (see STAR Methods). Immunization with the 20-mer still elicited a dominant response to the preF/postF-shared surface area (Figures S3D–S3H). These data demonstrate that the 20-mer can appreciably skew the specificity of vaccine-elicited antibodies, possibly through modulation of epitope accessibility by the dense and repetitive array of antigen.[17,18]

To address the question of epitope accessibility, we immunized macaques with a nanoparticle displaying half the copies of preF (10-mer) (Figure 3E), which should substantially alter the accessibility of several base-proximal epitopes. The 10-mer elicited only modest differences in the total magnitude of preF-binding and neutralizing antibodies (Figures 3F and 3G), consistent with data obtained using similar partial valency immunogens we previously evaluated in mice.[4] The proportion of antibodies binding to the preF/postF-shared surface area remained high with the 10-mer relative to the 1-mer (Figures 3H and S3B). Simultaneously, as hypothesized, the 10-mer slightly enhanced antibody reactivity to base-proximal epitopes such as the nanoparticle scaffold (Figure 3I) and the foldon trimerization domain (Figure 3J), suggesting increased accessibility relative to the 20-mer but not the 1-mer, where foldon-specific antibodies were most prominent. Assaying epitope accessibility by biolayer interferometry (BLI) showed reduced binding by foldon-specific antibodies to the assembled multivalent immunogens (Figure S3I), especially when accounting for the increased mass of the nanoparticles,[17,18] whereas binding to apex-proximal epitopes remained largely equivalent. Combined, the *in vivo* and *in vitro* results confirmed that valency differentially modulates epitope accessibility. Additionally, epitope mapping by competition with reference antibodies (listed in Figure 3A) further supported a skewing toward preF/postF-shared surface epitopes (i.e., antigenic sites I, II, III, and IV) by the 20-mer and 10-mer immunogens (Figures 3K, 3L, and S3J). Importantly, equivalent reactivity to the preF-specific apex epitope (i.e., site Ø) was induced by all three immunogens. A multidimensional scaling projection of the epitope-specificity profile of each animal's plasma partially separated the three immunogen groups after B2 (Figure 3M). Thus, we concluded that antigen display valency can modulate the specificities of vaccine-elicited antibodies through decreased accessibility of primarily base-proximal epitopes.

Antigenicity is coupled to antigen conformation

Both the 20-mer and 10-mer induced substantial antibody responses specific to antigenic site I, located at the base of preF and apex of postF, which suggested that both preF and postF conformations may have been present on the nanoparticle immunogens. Indeed, negative-stain electron microscopy (nsEM) of the non-assembled antigen-bearing nanoparticle component (DS-Cav1-I53-50A) revealed two distinct conformations reminiscent of preF and postF, with most (~86%) of the component
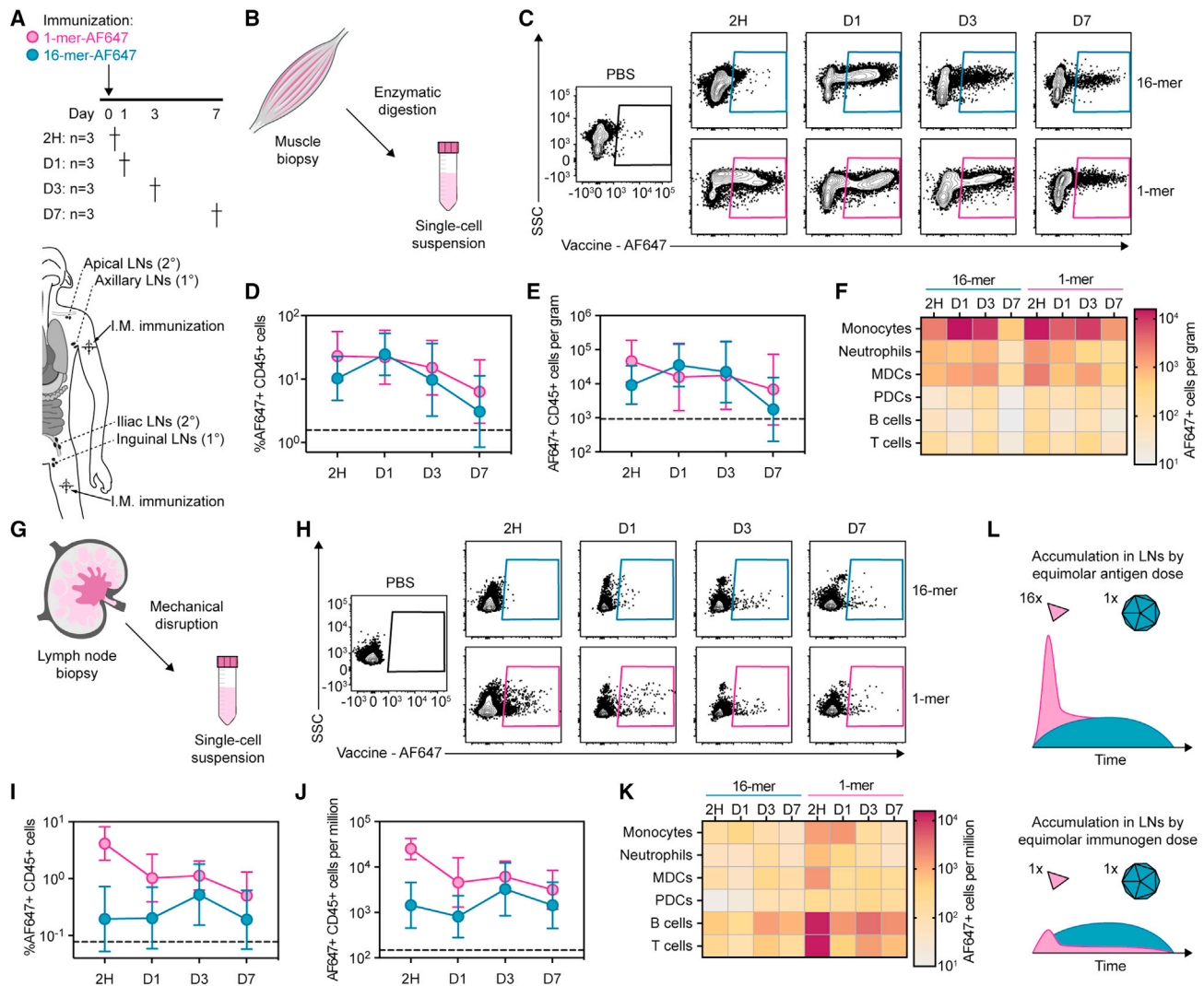
Figure 2. Larger size of multivalent nanoparticles delays kinetics of lymph node accumulation

(A) Naive rhesus macaques were immunized with fluorescently labeled (AF647) 1-mer or 16-mer immunogens in SWE adjuvant by intramuscular (I.M.) administration. PBS injections in the calf muscle served as internal controls. At set time points after administration (n = 3 animals per time point), the animals were euthanized, and tissues were harvested. Shown is a schematic of the experimental design for longitudinal analysis of vaccine trafficking kinetics as well as a depiction of immunization sites and the corresponding draining lymph nodes (LNs).

(B) Schematic of muscle biopsy processing by enzymatic digestion to single-cell suspension for flow cytometry analysis.

(C) Representative flow cytometry plots of AF647+ signal within CD45+ cells in muscle at the analyzed time points.

(D and E) Longitudinal quantification of AF647+ CD45+ cells as a percentage of CD45+ cells (D) or as per gram of muscle tissue (E).

(F) Heatmap of AF647+ CD45+ immune cell subsets per gram of muscle tissue over time. MDCs, myeloid dendritic cells; PDCs, plasmacytoid dendritic cells.

(G) Schematic of lymph node biopsy processing by mechanical disruption to single-cell suspension for flow cytometry analysis.

(H) Representative flow cytometry plots of AF647+ signal within CD45+ cells in secondary (2°) draining LNs (i.e., apical or iliac LNs) at the analyzed time points.

(I and J) Longitudinal quantification of AF647+ CD45+ cells in 2° draining LNs as a percentage of CD45+ cells (I) or as per million cells used for analysis (J).

(K) Heatmap of AF647+ CD45+ immune cell subsets per million cells in 2° draining LNs over time.

(L) Summary schematic of *in vivo* immunogen trafficking results by immunogen load vs. by antigen load.

(D, E, I, and J) Geometric mean and geometric SD displayed of individual tissue samples (n = 4–6 samples per group per time point). Dotted line represents the limit of detection based on PBS controls. Statistical significance was assessed by two-tailed Mann-Whitney U test with a false discovery rate correction for multiple comparisons. (F and K) Geometric mean displayed (n = 4–6 samples per group per time point).

See also Figure S2.

particles classified in the postF conformation (Figures 4A and 4B). This was further validated by detectable binding of the postF-specific antibody 4D7 to both postF and DS-Cav1-I53-50A, but not to preF (DS-Cav1), by nsEM and BLI (Figures S3K and S3L). Co-display of both preF and postF conformations on the multivalent nanoparticles was confirmed by sandwich ELISAs that captured postF with 4D7 or preF with D25 (Figure 4C). Thus, the overrepresentation of antibodies binding the
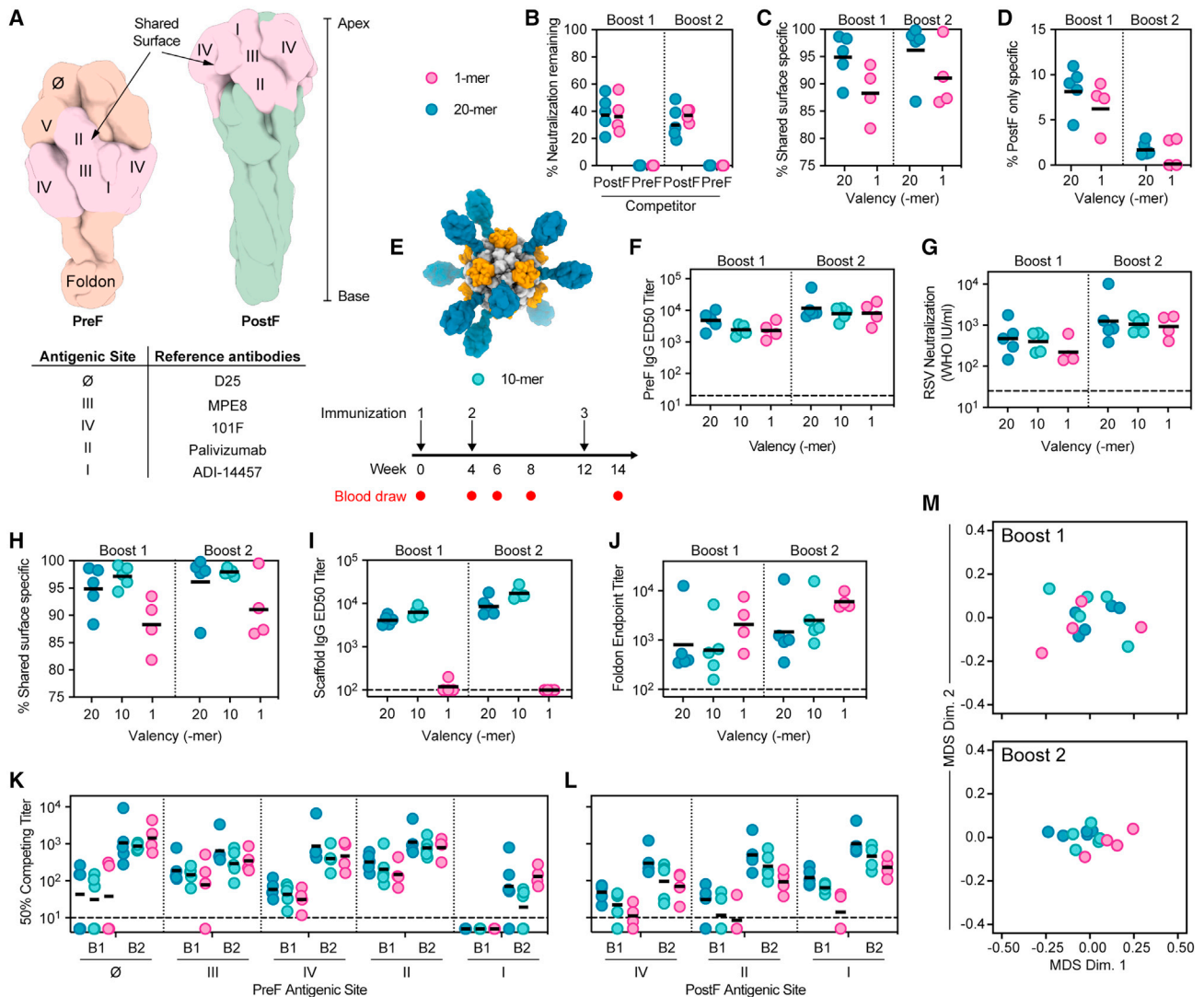
Figure 3. Valency-dependent skewing of serum antibody specificities

(A) Models of preF (DS-Cav1; PDB: 4mmv) and postF (PDB: 3rrr) colored by unique (preF, orange; postF, green) and preF/postF shared surface area (pink). Antigenic sites are labeled in the models, and corresponding reference monoclonal antibodies used for epitope mapping in (K)–(M) are listed in the table.

(B) Proportion of RSV neutralization in serum that remains after competition with excess postF or preF.

(C) Proportion of preF binding titer in plasma that is outcompeted by excess postF.

(D) Proportion of postF binding titer in plasma that remains after competition with excess preF.

(E–M) Naive rhesus macaques (n = 5) were immunized by intramuscular injection with a 10-mer immunogen in SWE adjuvant at weeks 0, 4, and 12 as depicted in (E).

(F) PreF-binding IgG titers of plasma measured after boost 1 and boost 2.

(G) RSV neutralization of sera measured after boost 1 and boost 2.

(H) Proportion of preF binding titer in plasma that is outcompeted by excess postF after boost 1 and boost 2.

(I) I53-50 nanoparticle scaffold-binding IgG titers of plasma measured after boost 1 and boost 2.

(J) Foldon-binding IgG titers of plasma measured after boost 1 and boost 2.

(K and L) Plasma dilution that competes 50% of reference antibody binding to indicated antigenic sites on preF (K) or postF (L). Site Ø (D25), site III (MPE8), site IV (101F), site II (palivizumab), and site I (ADI-14457).

(M) Multidimensional scaling projection of plasma epitope reactivity as measured by reference antibody competition.

(B–M) Bars depict geometric mean. Data points represent individual animals (n = 4–5 per group). Statistical significance was assessed by two-tailed Mann-Whitney U test with a false discovery rate correction for multiple comparisons.

See also Figure S3.

preF/postF-shared surface area induced by both the 20-mer and 10-mer is likely best explained by the co-display of both preF and postF antigens (Figure 4D).

To address the effect of the postF conformation on antibody responses, we analyzed the polyclonal antibody specificities from macaques immunized twice with 1-mer postF and once
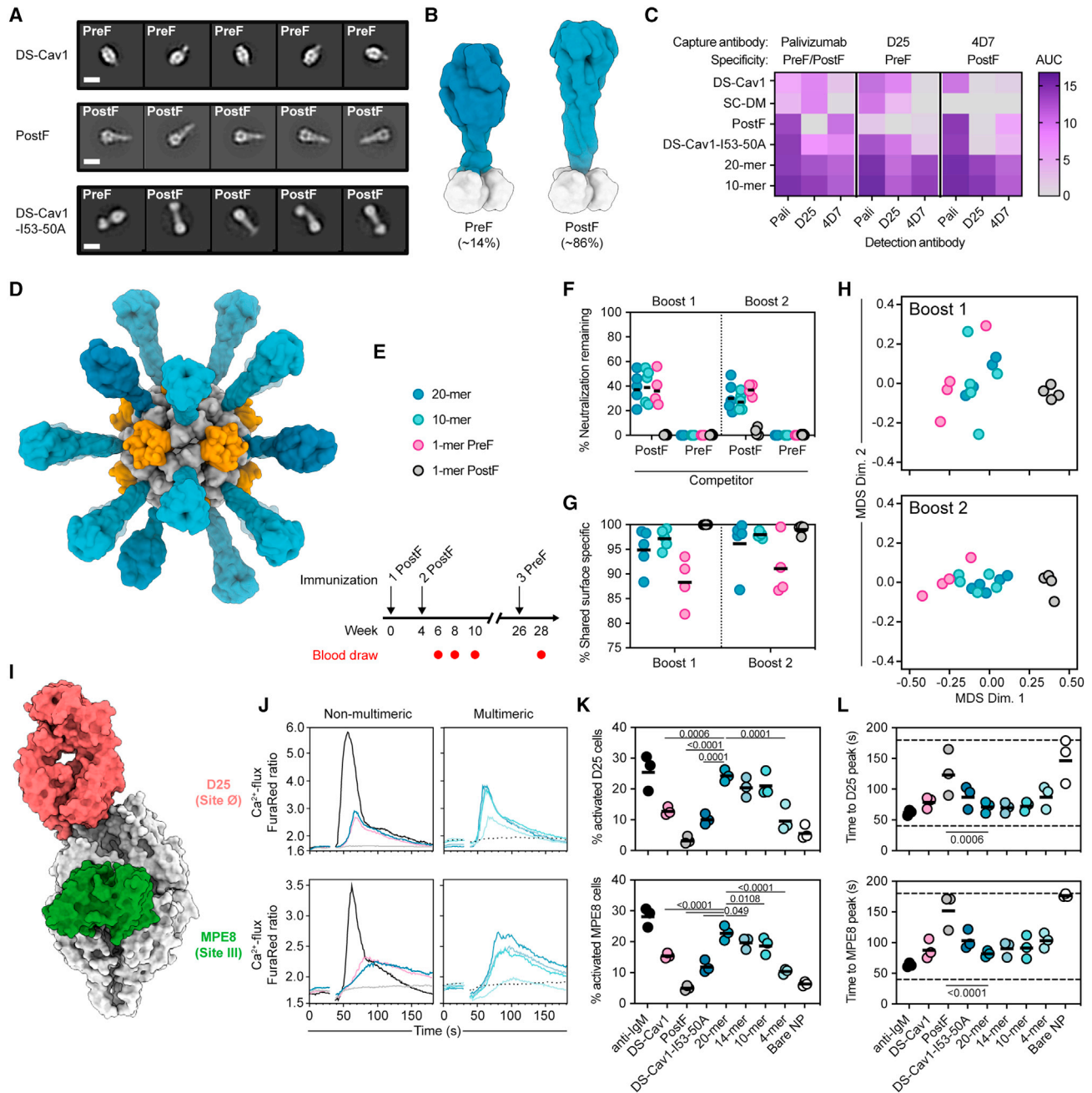
Figure 4. Conformation- and valency-dependent activation of B cells

(A) Two-dimensional classifications of negative-stain electron microscopy (nsEM) particles of DS-Cav1, postF, and DS-Cav1-I53-50A. Classes are labeled by their conformation based on the characteristic lollipop shape of postF and the oval shape of preF. Scale bars, 10 nm.

(B) Proportions of DS-Cav1-I53-50A component in preF or postF conformation from nsEM analysis with corresponding models. A total of 10,657 particles were analyzed.

(C) Area under the curve (AUC) quantification of sandwich ELISAs with capture of immunogens using the antibodies palivizumab (preF/postF-specific), D25 (preF-specific), or 4D7 (postF-specific). Detection was performed with biotinylated versions of the same antibodies. Representative data from two independent experiments.

(D) Updated model of 20-mer nanoparticle co-displaying preF and postF at 15% and 85%, respectively.

(E–H) Naive rhesus macaques (n = 4) were immunized by intramuscular injection with two doses of 1-mer postF immunogen in polyIC:LC adjuvant at weeks 0 and 4, and with one dose of 1-mer preF immunogen in polyIC:LC adjuvant at week 26 as depicted in (E). (F) Proportion of RSV neutralization in serum that remains after competition with excess postF or preF. (G) Proportion of preF-binding titer in plasma that is outcompeted by excess postF. (H) Multidimensional scaling projection of plasma epitope reactivity as measured by reference antibody competition.

(I) Structures of antibodies D25 (PDB: 4JHW) and MPE8 (PDB: 5U68) binding to preF.

(legend continued on next page)

with 1-mer preF in polyriboinosinic-polyribocytidylic acid (poly-IC:LC) adjuvant (Figure 4E).[23,38] Neutralizing antibodies were substantially lower in 1-mer postF animals compared with animals receiving only 1-mer preF in polyIC:LC adjuvant (Figure S3M) but recovered to similar levels with the 1-mer preF boost. Both the neutralizing and preF-binding responses were dominated by preF/postF-shared surface reactivity (Figures 4F, 4G, S3A, and S3B), although this remained distinct from the other immunization groups (Figures 4H, S3N, and S3O). In summary, the improved immunogenicity of the multivalent immunogens relative to 1-mer postF, as well as their distinct antibody profiles, strongly suggests that multimerization may have intrinsic effects on B cells that are independent of antigen conformation.

Valency-dependent avidity can overcome suboptimal antigenicity

To investigate the direct effects of antigen valency on B cell activation, we generated two RAMOS B cell lines bearing either the preF site Ø-specific antibody D25 or the preF site III-specific antibody MPE8 as functional membrane-bound IgM BCRs (Figure 4I). Antigen conformation and valency were separately assessed for activation, as measured by Ca^{2+}-flux, with multimeric and non-multimeric immunogens (Figures 4J–4L). A prominent valency-dependent avidity effect was observed in the activation of both cell lines, with multimeric immunogens (high avidity and low antigenicity) significantly improving activation compared with non-multimeric antigens (low avidity), but not the cell line reaction times, regardless of their intrinsic antigenicity (Figures 4K and 4L). The avidity advantage was lost when valency dropped to 20% (4-mer). Combined, these data pair well with the equivalent elicitation of D25- and MPE8-competing serum antibodies in immunized animals (Figures 3K and S3N). Thus, increased antigen display valency can overcome suboptimal antigenicity through improved avidity or BCR cross-linking on cognate B cells.

Multivalency increases clonal diversity of the B cell response

Elegant adoptive transfer mouse models have shown that the affinity threshold needed for activation and recruitment of B cells into GCs in vivo can effectively be lowered by increased avidity from multivalent display[39] and that this also leads to increased recruitment of diverse B cell affinities.[11] We hypothesized that this phenomenon could manifest in a quantifiable difference in the output of MBCs from the GC reaction. Simultaneously, we appreciated that epitope accessibility and antigen conformation may convolute the output of MBC specificities. We quantified the specificity distribution of circulating MBCs using fluorescent preF and postF probes (Figures 5A–5C and S4A–S4C), and these distributions were in line with our earlier serology analyses (Fig-

ure 4G). This confirmed a role for accessibility and conformation in B cell selection. Also, as hypothesized, a quantifiable 5- to 8-fold increase in the magnitude of preF/postF-shared surface area-specific B cells was evident in 20-mer animals compared with 1-mer animals, and this accounted for the roughly 2-fold increase in total F-specific B cells in the 20-mer group (Figures 5D and 5E). This suggests that multivalent display may modulate B cell recruitment on the epitope level and focus the response to the most prominently displayed (i.e., most accessible) epitopes—in this case, the preF/postF-shared surface area at the apex of the postF displayed on the 20-mer.

At the B cell level, epitope-focusing could be the result of two distinct scenarios: an oligoclonal response of narrow specificity or a highly polyclonal response of diverse specificities (Figure 5F). The latter scenario would indicate the recruitment of diverse B cell affinities. To distinguish between these possibilities, we set out to capture the composition of the expanded preF/postF-shared surface area-specific B cell pool (i.e., the epitope-focused B cells) by quantifying the clonotype diversity of the B cell repertoire. We combined single-cell BCR sequences of known specificity (~400 B cells per animal) with longitudinal bulk IgG repertoire sequencing datasets utilizing a previously described data integration approach (Figure 5G).[40] This yielded a total of ~190,000 F-specific BCR sequences at boost 1 (B1) and B2 (Figures 5G, 5H, and S4D–S4G). Large clonal expansions, as assessed by unique VDJ rearrangements, and increased frequency of SHM were evident at B2 relative to B1 (Figures 5E and S4H–S4L). Distinct usage of Ig heavy chain V (IGHV) and IGHJ alleles was evident by immunization group (Figure 5I), and the quantity of unique pairings differed significantly by specificity (Figure 5J). The estimated clonotype richness, assessed with both Chao1 and Recon, similarly showed significant differences by B cell specificity (Figures 5K and 5L). The increased detection of unique clonotypes confirms that the epitope-focusing observed in the preF/postF-shared surface area was driven by the activation and recruitment of a diversified pool of precursor B cells rather than an expansion of a narrow selection of B cells. Thus, multivalent display is likely lowering the affinity threshold needed for B cell activation in vivo in an avidity-dependent manner, as seen in vitro (Figures 4I–4L), and recruiting B cells of more diverse initial affinities, as shown previously in adoptive transfer mouse models.[11,39] These data also suggest that epitope accessibility may be tightly linked to epitope-focusing and the diversification of responding B cells.

Diverse B cell specificities exhibit potent neutralization

Next, we expressed 61 monoclonal antibodies to assess the functional relevance of epitope-focusing on a molecular level. The antibodies matched the specificities suggested by our sorting strategy (Figures S5A–S5D) and predominantly bound either

---

(J–L) Quantification of Ca^{2+}-flux from BCR-signaling in RAMOS cells transduced with D25 (top row) or MPE8 (bottom row) IgM BCRs. Cell lines were stimulated with different immunogens at 5 μg/mL concentrations of antigen (i.e., equimolar antigen doses) after reading a 30 s baseline. Representative plots of Ca^{2+}-flux over time are shown in (J) and data from three independent experiments is plotted as the proportion of activated cells (K) or the time to peak activation (L). Dotted lines in (L) show time point of reading after antigen addition (40 s) and total assay time (180 s). Anti-IgM stimulation was used as a positive control.
(F and G) Data points represent individual animals. Bars depict geometric mean. Statistical significance was assessed by two-tailed Mann-Whitney U test with a false discovery rate correction for multiple comparisons. (K and L) Data points represent independent experiments (n = 3). Bars depict geometric mean. Statistical significance was assessed by two-tailed repeated measures one-way ANOVA with Dunnett's multiple comparisons test against the 20-mer immunogen.
See also Figure S3.
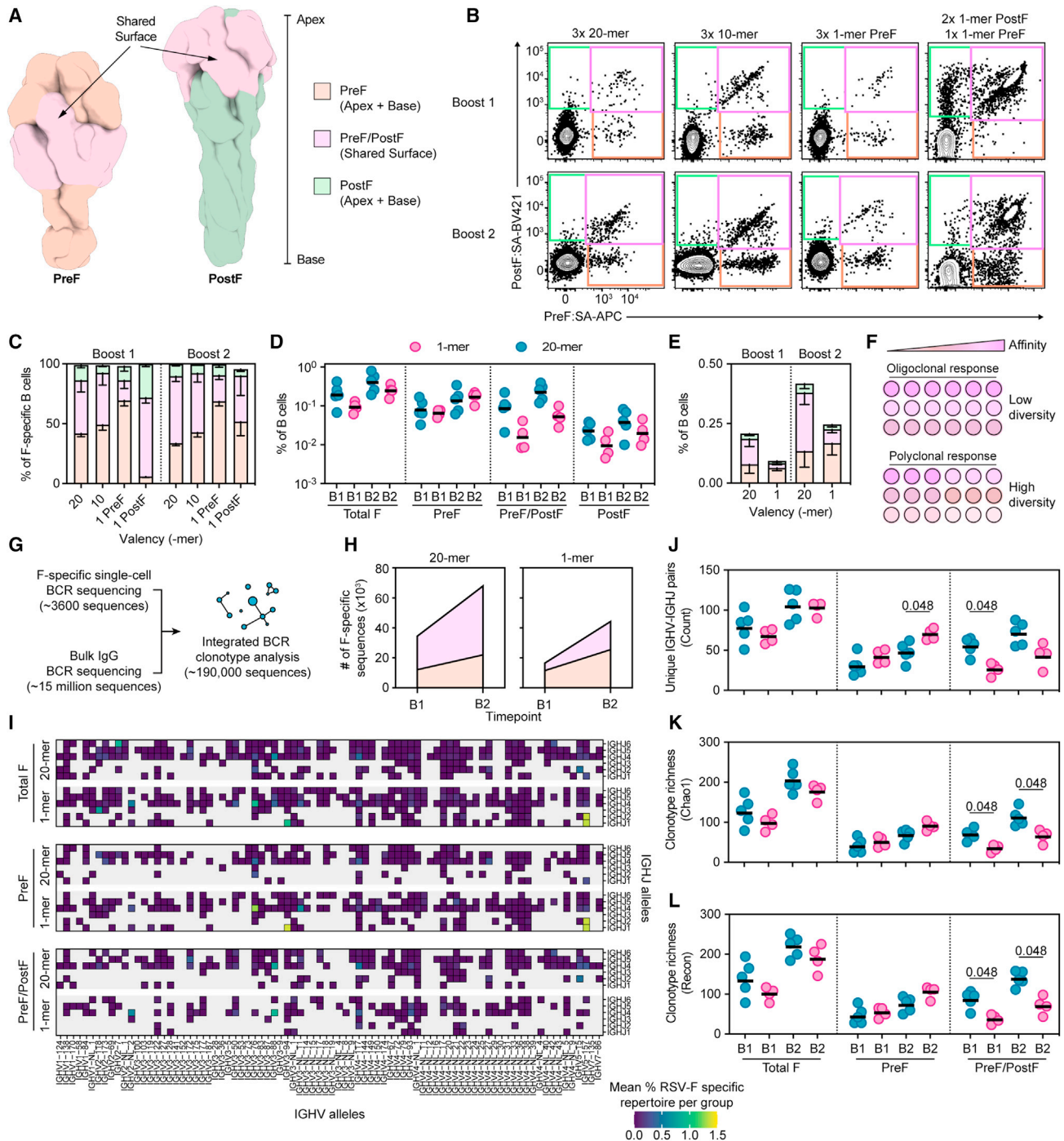
Figure 5. Multivalency increases clonal diversity of the B cell response

(A) Models of preF (DS-Cav1; PDB: 4mmv) and postF (PDB: 3rrr) antigens used for probing memory B cells. Antigens are colored by unique (preF: orange; postF: green) and preF/postF-shared surface area (pink) as in gates in (B).

(B) Representative flow cytometry plots of preF and postF probing specificities of IgG+ memory B cells per immunogen group from boost 1 (week 6 for postF group; week 8 for rest) and boost 2 (2 weeks after immunization) samples.

(C) Proportion of total F-specific memory B cells by specificity per immunogen group at boost 1 and boost 2.

(D and E) Quantification of F-specificity as a proportion of total B cells for 20-mer and 1-mer immunogen groups as individual data points per animal (D) or as a geometric mean aggregate (E).

(F) Cartoon depicting the two possible clonotype responses driving a focused expansion of B cells. Either an oligoclonal response of low clonotype diversity with high initial affinity or a polyclonal response of high clonotype diversity with a variety of initial affinities, including low-affinity cells.

(legend continued on next page)

preF or both preF and postF (Figure 6A). Diverse epitopes on the F protein were targeted, including all known antigenic sites (i.e., Ø, I, II, III, IV, and V), the foldon trimerization domain, and previously unmapped sites, as determined by epitope binning (Figures 6B, 6C, and S5E) and confirmed by nsEM (Figures 6D, 6E, and S6). We suspected that some unmapped antibodies may bind epitopes in the preF trimer interface that become surface-exposed in the postF conformation, of which a subset could be shown to bind to surface epitopes on postF, but not preF, when analyzed by nsEM (Figure S6J). Both the 20-mer and 1-mer immunogens elicited antibodies with a wide range of neutralization potencies and specificities (Figures 6F and 6G). At the epitope level, neutralization potency largely followed the established sensitivity hierarchy (Figures 6B and 6C),[28] and no associations between clonal expansion, SHM, fragment antigen-binding (Fab) affinity, or potency were evident (Figures 6H and S5F–S5K). Reverting 16 antibodies to their germline precursor state (unmutated common ancestor [UCA]) and assaying for monovalent Fab affinity or bivalent IgG affinity showed that only three had detectable affinity as Fabs, whereas nine did as bivalent IgGs (Figure 6I). Thus, many antibodies may derive from precursor B cells of low affinity that benefit from increased avidity for initial recruitment into the GC response.

Broad and ultrapotent antibodies affinity mature from low-affinity precursor B cells

We hypothesized that diversifying the B cell pool through the recruitment of low affinity, and possibly rare, precursor B cells may increase the probability that affinity maturation produces antibodies with extreme potency or even breadth. Hence, we more closely examined the affinity maturation of 20-mer-elicited antibodies binding the epitope-focused and clonally diversified preF/postF-shared surface area.

The site II-specific antibody LOR21 stood out as an exception to the established neutralization sensitivity hierarchy, with 20-fold higher potency than the clinically used and prototypic site II-specific antibody palivizumab (Figure 7A). A low-resolution 3D reconstruction of the LOR21 Fab:preF complex obtained by nsEM confirmed a similar binding orientation to the site II-directed antibody motavizumab, a derivative of palivizumab (Figure 7B). Reversion of LOR21 to its UCA revealed that potency was acquired through extensive SHM (Figures 7A, 7C, and S7A). Although the UCA could neutralize RSV, it did not have a detectable affinity to preF as a Fab (Figure 7D). As a bivalent IgG, the UCA had a detectable affinity to both preF and postF (Figure 7E), suggesting avidity from the 20-mer may enhance the activation of this precursor B cell. LOR21 is thereby an example of an ultrapotent neutralizing antibody whose affinity matures from a low-affinity precursor B cell.

Antigenic sites III and IV, within the preF/postF-shared surface area (Figure 6B), can elicit antibodies with the capacity to cross-neutralize the related human metapneumovirus (MPV) through limited patches of high conservation.[41–43] Of our 61 antibodies, four antibodies cross-reacted with the F protein of MPV (Figure S7B) and two antibodies could also neutralize MPV (Figure S7C). The cross-neutralizing antibody LOR24 (Figure 7F) was mapped to the conserved antigenic site III (Figure S5E) and bound with a distinct binding mode relative to the prototypic site III-specific cross-neutralizing antibody MPE8 as observed in a low-resolution 3D reconstruction by nsEM (Figure 7G). The LOR24 antibody affinity matured to acquire detectable RSV preF affinity, RSV neutralization, and MPV cross-neutralization (Figures 7F, 7I, and 7J), whereas a clonally related antibody, LOR19, affinity matured down a different path and did not acquire MPV cross-neutralization (Figures 7H–7J and S7D). Additionally, a LOR24-related lineage was found through a sequence identity search in a separate 20-mer animal (Figure S7E). Expression of the natively paired heavy and light chain, LOR74, and an affinity-matured variant, LOR74_mut, revealed that this lineage also acquired MPV cross-neutralization through affinity maturation (Figures 7J, S7F, and S7G). Although affinity to preF was undetectable for the UCA, affinity for postF was measurable (Figure 7K). Consequently, low but consistently detectable activation of a LOR24_UCA BCR RAMOS cell line was measured for 1-mer postF as well as the 20-mer and 10-mer immunogens (Figures 7L and 7M). Importantly, the antigen-bearing nanoparticle component, DS-Cav1-I53-50A, showed significantly lower activation of the UCA cell line, which indicated a strong avidity-dependent activation from the multivalent immunogens. Thus, the elicitation of MPV cross-neutralizing antibodies through homologous RSV prime-boost immunization in naive animals may benefit from the enhanced avidity of multivalent display.

Assessment of serum MPV neutralization showed a detectable response in all 10-mer animals but only in two 20-mer and two 1-mer preF animals (Figure 7N). Improved elicitation of cross-reactive responses may therefore require both increased avidity and increased epitope accessibility, especially for targeting the conserved antigenic site III. In summary, we conclude that multivalent display enables the recruitment of low-affinity B cells of diverse specificities and potencies, with some developing unusually high potency or neutralization breadth through affinity maturation.

DISCUSSION

Structure-based vaccine design is transforming vaccinology by improving the elicitation of neutralizing antibodies against a multitude of viral protein subunit antigens.[22] The display of these

(G–L) The BCRs of single-cell sorted F-specific B cells as in (B) were sequenced from 20-mer and 1-mer immunogen groups at boost 2 (∼400 cells per animal). These sequences were integrated with bulk BCR sequencing of PBMCs from boost 1 and boost 2 time points (∼0.5–1.3 million per animal). Clonotype clustering with F-specific single cells was used to identify related sequences in the bulk BCR datasets (∼190,000 sequences). An overview of the integrated clonotype analysis approach combining single-cell and bulk BCR sequencing datasets is shown in (G). (H) Sum of preF- and preF/postF-shared surface-specific sequences identified at boost 1 and boost 2 time points. (I) Heatmap of mean paired IGHV-IGHJ allele usage of the RSV-F-specific repertoire combined for boost 1 and boost 2 time points. (J) Number of unique IGHV-IGHJ allele pairs used per animal, split by time point and specificity of clonotypes. (K and L) Repertoire diversity assessed by species richness estimators Chao1 (K) or Recon (L), split by time point and specificity of clonotypes.

(C–L) Bars depict geometric mean, and error bars are geometric SD. Data points represent individual animals. Statistical significance was assessed by two-tailed Mann-Whitney U test with a false discovery rate correction for multiple comparisons.

See also Figure S4.
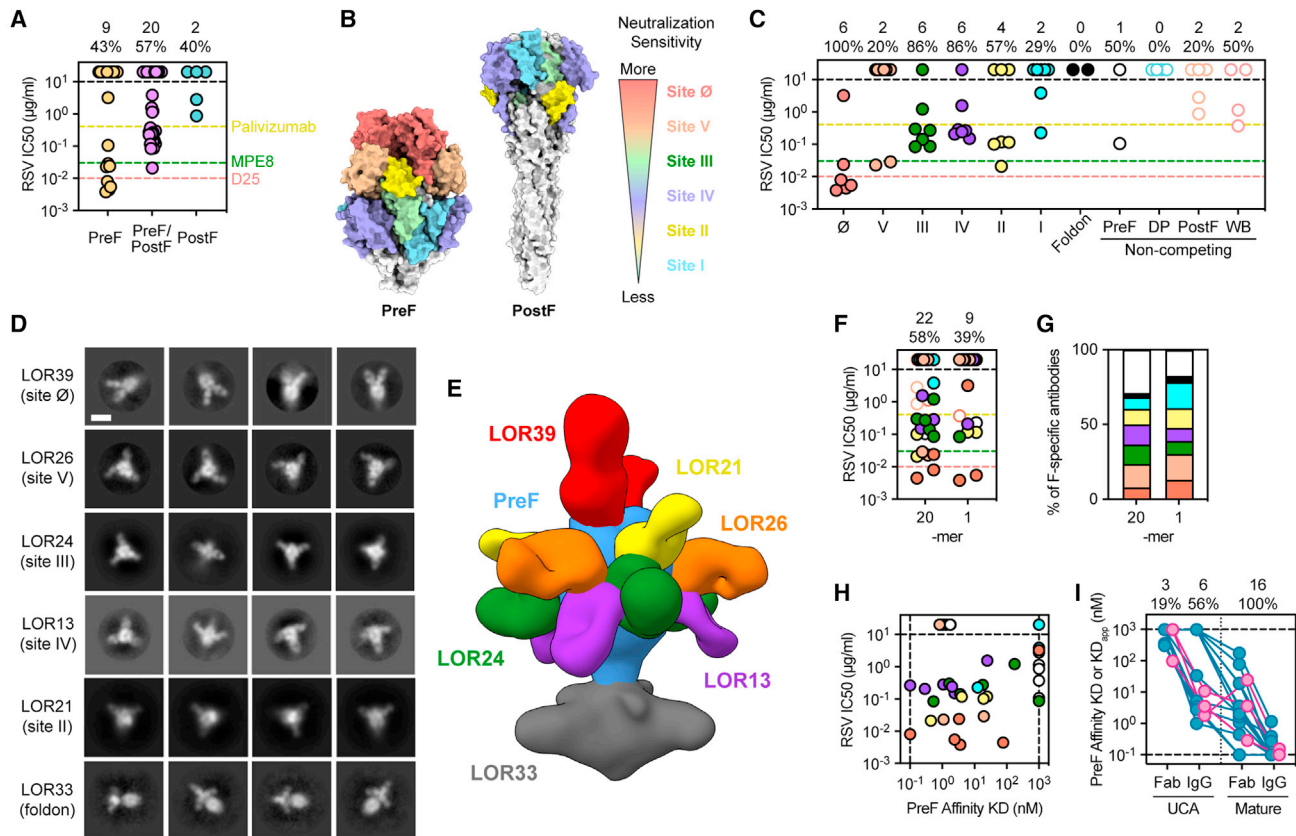
Figure 6. Diverse B cell specificities exhibit potent neutralization

(A) RSV neutralization potency of characterized monoclonal antibodies (n = 61) plotted according to their binding specificity to preF-only (n = 21), both preF and postF (preF/postF; n = 35), or postF-only (n = 5) by ELISA. Colored dotted lines denote the IC50 values of the reference antibodies palivizumab (yellow), MPE8 (green), and D25 (red) run in the same assay. The number of neutralizing antibodies (top) and the percentage of analyzed antibodies that are neutralizing (bottom) per specificity is displayed.

(B) Models of preF (DS-Cav1; PDB: 4mmu) and postF (PDB: 3rrr) colored by defined antigenic sites. The established neutralization sensitivity hierarchy is also pictured.

(C) RSV neutralization potency by epitope specificity of antibodies (n = 61). Non-competing antibodies are classified based on their preferential binding to preF, preF/postF (DP), or postF. WB denotes weak binders to both preF and postF. The number of neutralizing antibodies (top) and the percentage of analyzed antibodies that are neutralizing (bottom) per specificity is displayed.

(D) nsEM 2D class-averages of representative Fabs binding distinct antigenic sites on preF. Scale bars, 10 nm.

(E) Composite 3D reconstruction demonstrating the binding of representative Fabs to preF (blue) from (D).

(F) RSV neutralization potency of antibodies by vaccine group (n = 38 for 20-mer; n = 23 for 1-mer). Colored by site specificity as in (C).

(G) Epitope specificity of antibodies by vaccine group as a proportion of total F-specific antibodies. Colored by site specificity as in (C).

(H) Fab affinity to preF plotted against RSV neutralization of antibodies (n = 61). Colored by site specificity as in (C).

(I) Fab affinity and IgG apparent affinity measured by BLI against preF for unmutated common ancestor (UCA) and mature antibody pairs (n = 16 pairs). Dots colored by vaccine group: 20-mer (blue; n = 13) and 1-mer (pink; n = 3). The number of antibodies with detectable affinities (top) and as a percentage of analyzed antibodies (bottom).

(A, C, F, H, and I) Data points represent individual IgG antibodies or Fab fragments thereof. Black-dotted lines represent the limits of detection of the assay (lower and/or upper limit).

See also Figures S5 and S6.

antigens on multivalent nanoparticles is an essential extension of this design approach that can modulate off-target responses characteristic of the intrinsic immunodominance hierarchy of viral antigens. Here, we have shown that several features of nanoparticle immunogens can influence the magnitude and quality of vaccine-elicited antibodies, providing important information that will guide future nanoparticle vaccine design efforts.

Using a multifaceted approach, we performed an in-depth study of the B cell response elicited in rhesus macaques to RSV preF (DS-Cav1) immunization as a 1-mer and when dis-

played as a 20-mer or 10-mer on the designed two-component nanoparticle I53-50.[4] We showed that humoral responses may be modulated by two interrelated aspects of the nanoparticle immunogen: its size and valency. Nanoparticle display delayed the kinetics of antigen accumulation in LNs, which has previously been associated with increases in vaccine-elicited antibody titers and GC responses.[5,6,33] In our study, increases in humoral responses induced by the 20-mer over the 1-mer were most prominent in the B cell compartment across multiple tissues. Furthermore, the equivalent magnitude of responses elicited
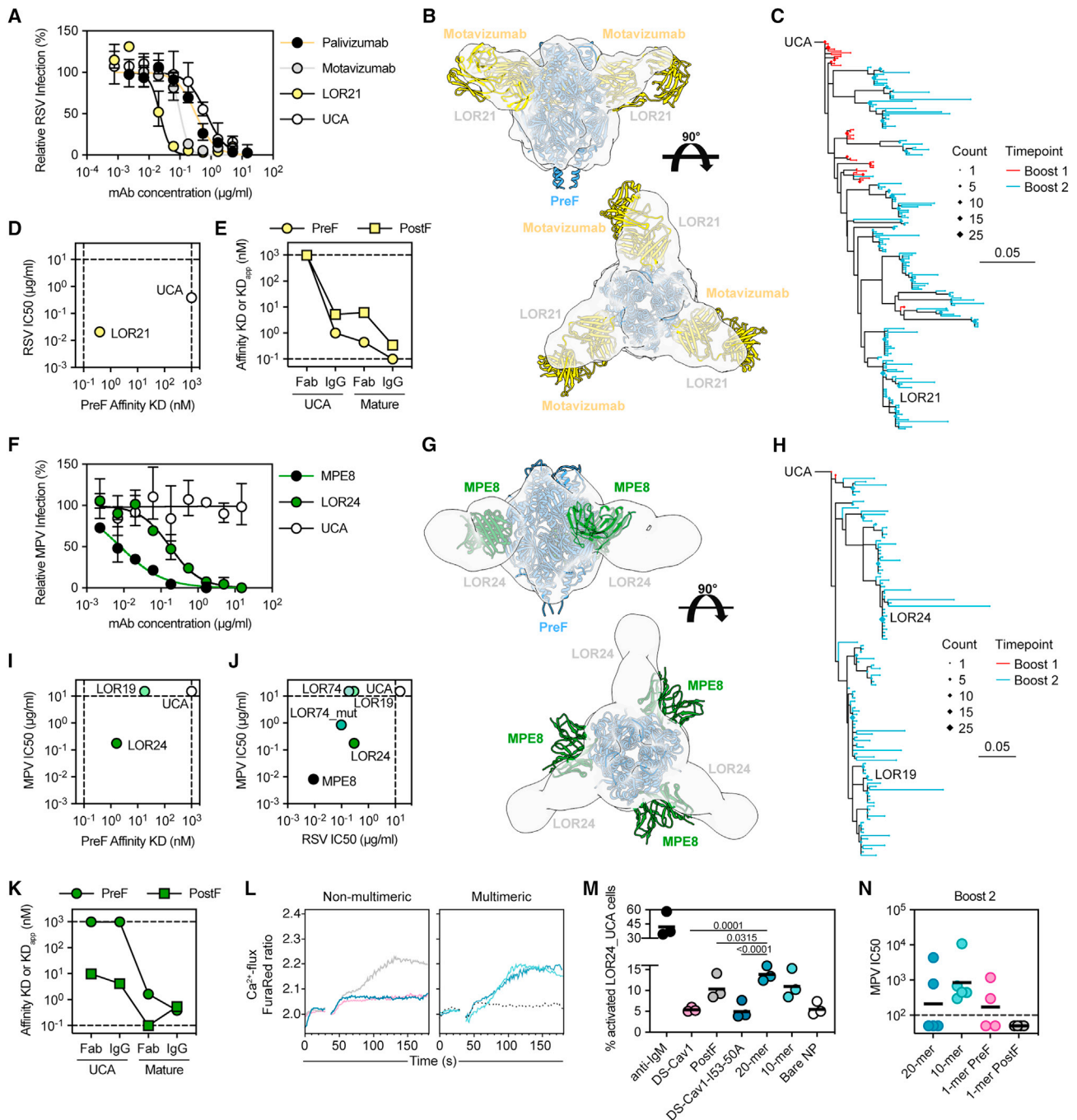
Figure 7. Broad and ultrapotent antibodies affinity mature from low-affinity precursor B cells

(A) RSV neutralization curves for LOR21 and its germline precursor (UCA, unmutated common ancestor). For reference, the site II-specific antibodies palivizumab and motavizumab are shown.

(B) nsEM density map of LOR21 Fab:preF complex superimposed with the structure of site II-specific antibody motavizumab (PDB: 4ZYP).

(C) Clonal lineage tree for the heavy chain of the LOR21 clonotype. Tree branches are colored by the sampling time point, and nodes are sized by sequence count. n = 477 sequences.

(D) Fab affinity to preF plotted against RSV neutralization for the IgG of LOR21 and its UCA.

(E) Fab affinity and IgG apparent affinity measured against preF and postF for the UCA and mature LOR21 antibody.

(F) MPV neutralization curves for LOR24 and its UCA. For reference, the site III-specific antibody MPE8 is shown.

(G) nsEM density map of LOR24 Fab:preF complex superimposed with the structure of site III-specific antibody MPE8 (PDB: 5U68).

(H) Clonal lineage tree for the heavy chain of the LOR24 clonotype. The clonally related antibody LOR19 is also shown. Tree branches are colored by the sampling time point, and nodes are sized by sequence count. n = 224 sequences.

(I) Fab affinity to RSV preF plotted against MPV neutralization for LOR24, LOR19, and their UCA.

(legend continued on next page)

by the 20-mer and 10-mer immunogens suggests that nanoparticle size may have the largest effect on the magnitude of B cell responses at certain valencies and that the nanoparticles remain oligomeric *in vivo*, in line with their high stability *in vitro*.[4,17,19,44] Differences between 20-mer and 10-mer immunogens were instead largely represented by skewing of the epitope specificities of the antibody and B cell response, likely because of differential accessibility of base-proximal epitopes. However, the DS-Cav1 displayed on the nanoparticles adopted both the preF and postF conformations, which also had a significant impact on specificity skewing. Future efforts could benefit from utilizing more conformationally stable preF constructs,[45–47] which is the case for the vaccine candidate under clinical development based on this work. Importantly, increased antigen valency provided an avidity effect that efficiently activated B cells despite suboptimal antigenicity on the multivalent immunogens.

The increased avidity attributed to multivalent display supports the seeding of GCs by a diverse pool of B cells with wide-ranging affinities and genetic properties through lowering the threshold for activation and recruitment. This is well in line with GC entry primarily being limited by competition[39,48–50] and is supported by previous observations of the frequent presence of low-affinity B cells in GCs.[11,50–52] Our observation of a more diverse output of MBCs after 20-mer immunization suggests that avidity may play a significant role in the activation and selection of B cells *in vivo*. Recent detailed studies in mouse models have also identified profound effects of antigen valency on cognate B cell recruitment to GC responses, including the recruitment of diverse affinities.[11] This diversity increases the probability that one or more clones may develop unusual potency and/or even breadth later in the response or upon rechallenge. Notably, we isolated from 20-mer-immunized animals an unusually potent site II-specific antibody, LOR21, and two MPV cross-neutralizing antibodies, LOR24 and LOR74_mut. We found that these antibody lineages acquired their potency or breadth through affinity maturation and that their germline precursors had a low or undetectable affinity for the immunogen, highlighting a role for the avidity-dependent diversification of the B cell response. In a similar fashion, co-display of diverse influenza or coronavirus antigens has shown promise in inducing broad antibody responses in animal models.[21,53,54] We therefore speculate that epitope-focusing toward conserved epitopes between RSV-F and MPV-F may be further enhanced through optimization of antigen display geometry and the co-display of improved preF constructs of both RSV-F and MPV-F.[55,56]

In conclusion, multivalent display is a powerful means of recruiting a diversified and improved B cell response, both qualitatively and quantitatively. Designed nanoparticle scaffolds offer a versatile platform for control of antigen valency and the geometry of multivalent display. This should enable future systematic studies to further optimize multivalent display for the explicit targeting of select epitopes of interest on complex protein antigens to induce broad and ultrapotent neutralizing antibodies. Thus, the structural correlates of immunogenicity may be further defined through future in-depth studies of the genetic, biochemical, and structural properties of the induced polyclonal B cell response.

Limitations of the study

A major limitation of this study is the presence of distinct antigen conformations (i.e., preF and postF) on the multivalent nanoparticles. Importantly, the antigen conformation is unlikely to affect the trafficking characteristics of the immunogen, the accessibility of most base-proximal epitopes (except site I), and the relative accessibility of the preF/postF-shared surface area between multimerized and non-multimerized immunogens. Therefore, we hypothesize that multivalent display of only the preF conformation would similarly focus the B cell response to the apex of the preF conformation (i.e., antigenic sites Ø and V) rather than the preF/postF-shared surface area that is at the apex of the postF conformation. This interpretation follows the epitope accessibility hierarchy (i.e., apex is most accessible), evident here and in studies by others.[17,18,57] Thus, increased B cell diversity would remain the most likely outcome of an epitope-focused response resulting from multivalent display. Corroborating these results with preF or independently with the display of other antigens on multivalent nanoparticles in combination with deep analysis of the antigen-specific B cell repertoire will be important to pursue.

STAR★METHODS

Detailed methods are provided in the online version of this paper and include the following:

- KEY RESOURCES TABLE
- RESOURCE AVAILABILITY
  - Lead contact
  - Materials availability
  - Data and code availability
- EXPERIMENTAL MODEL AND STUDY PARTICIPANT DETAILS

(J) RSV neutralization plotted against MPV neutralization for LOR24, LOR19, and their UCA as well as the independent LOR24-lineage antibodies from a different animal: LOR74 and LOR74_mut. MPE8 is shown for reference.

(K) Fab affinity and IgG apparent affinity measured against preF and postF for the UCA and mature LOR24 antibody.

(L and M) Quantification of Ca^{2+}-flux from BCR-signaling in RAMOS cells transduced with the LOR24 UCA IgM BCR. The cell line was stimulated with different immunogens at 5 μg/mL concentrations of antigen (i.e., equimolar antigen doses) after reading a 30 s baseline. Representative plots of Ca^{2+}-flux over time are shown in (L), and data from three independent experiments is plotted as the proportion of activated cells (M). Anti-IgM stimulation was used as a positive control.

(N) MPV neutralization potency of plasma from immunized animals at boost 2 (2 weeks after third immunization).

(A, D–F, and I–K) Data points represent individual IgG antibodies or Fab fragments thereof. Black-dotted lines represent the limits of detection of the assay.

(M) Data points represent independent experiments (n = 3). Bars depict geometric mean. Statistical significance was assessed by two-tailed repeated measures one-way ANOVA with Dunnett's multiple comparisons test against the 20-mer immunogen.

(N) Data points represent individual animals (n = 4–5 per group). Bars show geometric mean. Statistical significance was assessed by a two-tailed Kruskal-Wallis test with Dunn's multiple comparisons test.

See also Figure S7.

SUPPLEMENTAL INFORMATION

Supplemental information can be found online at https://doi.org/10.1016/j.immuni.2023.08.011.

AUTHOR CONTRIBUTIONS

Conceptualization, S.O., N.P.K., and K. Loré; methodology, all authors; formal analysis, S.O., K. Lenart, R.A.C., M.C.M., N.B., J.K., R.S., A.P., and A.J.B.; investigation, S.O., K. Lenart, R.A.C., M.C.M., N.B., J.K., M. Corcoran, R.S., A.P., A.C., B.F., S.W., J.M., F.H., E.A.T., A.L., F.G., A.K., M. Chen, G.E.P., and A.J.B.; writing – original draft, S.O., N.P.K., and K. Loré; writing – review & editing, all authors; visualization, S.O., R.A.C., and A.J.B.; supervision, A.J.B., B.S.G., L.P., G.B.K.H., T.J.R., N.P.K., and K. Loré; funding acquisition, N.P.K. and K. Loré.

DECLARATION OF INTERESTS

N.P.K., B.F., L.P., and J.M. are named as inventors on patent applications filed by the University of Washington related to the data presented in this work. N.P.K. is a co-founder and shareholder in Icosavax, a company that has licensed the patent applications, and is a member of Icosavax's Scientific Advisory Board. The King lab has received unrelated sponsored research agreements from Pfizer and GSK. B.S.G. is an inventor on patents for the stabilization of the RSV-F protein (WO2014160463A1, preF RSV-F proteins and their use).

INCLUSION AND DIVERSITY

We support inclusive, diverse, and equitable conduct of research.

REFERENCES

1. Plotkin, S.A. (2010). Correlates of protection induced by vaccination. Clin. Vaccine Immunol. *17*, 1055–1065. https://doi.org/10.1128/CVI.00131-10.

2. Bachmann, M.F., and Jennings, G.T. (2010). Vaccine delivery: a matter of size, geometry, kinetics and molecular patterns. Nat. Rev. Immunol. *10*, 787–796. https://doi.org/10.1038/nri2868.

3. Victora, G.D., and Nussenzweig, M.C. (2012). Germinal centers. Annu. Rev. Immunol. *30*, 429–457. https://doi.org/10.1146/annurev-immunol-020711-075032.

4. Marcandalli, J., Fiala, B., Ols, S., Perotti, M., de van der Schueren, W.d.v.d., Snijder, J., Hodge, E., Benhaim, M., Ravichandran, R., Carter, L., et al. (2019). Induction of potent neutralizing antibody responses by a designed protein nanoparticle vaccine for respiratory syncytial virus. Cell *176*, 1420–1431.e17. https://doi.org/10.1016/j.cell.2019.01.046.

5. Zhang, Y.-N., Lazarovits, J., Poon, W., Ouyang, B., Nguyen, L.N.M., Kingston, B.R., and Chan, W.C.W. (2019). Nanoparticle size influences antigen retention and presentation in lymph node follicles for humoral immunity. Nano Lett. *19*, 7226–7235. https://doi.org/10.1021/acs.nanolett.9b02834.

6. Zinkhan, S., Ogrina, A., Balke, I., Reseviča, G., Zeltins, A., de Brot, S.d., Lipp, C., Chang, X., Zha, L., Vogel, M., et al. (2021). The impact of size on particle drainage dynamics and antibody response. J. Control. Release *331*, 296–308. https://doi.org/10.1016/j.jconrel.2021.01.012.

7. Tokatlian, T., Read, B.J., Jones, C.A., Kulp, D.W., Menis, S., Chang, J.Y.H., Steichen, J.M., Kumari, S., Allen, J.D., Dane, E.L., et al. (2019). Innate immune recognition of glycans targets HIV nanoparticle immunogens to germinal centers. Science *363*, 649–654. https://doi.org/10.1126/science.aat9120.

8. Reddy, S.T., van der Vlies, A.J.v.d., Simeoni, E., Angeli, V., Randolph, G.J., O'Neil, C.P., Lee, L.K., Swartz, M.A., and Hubbell, J.A. (2007). Exploiting lymphatic transport and complement activation in nanoparticle vaccines. Nat. Biotechnol. *25*, 1159–1164. https://doi.org/10.1038/nbt1332.

9. Kelly, H.G., Tan, H.-X., Juno, J.A., Esterbauer, R., Ju, Y., Jiang, W., Wimmer, V.C., Duckworth, B.C., Groom, J.R., Caruso, F., et al. (2020). Self-assembling influenza nanoparticle vaccines drive extended germinal center activity and memory B cell maturation. JCI Insight *5*, e136653. https://doi.org/10.1172/jci.insight.136653.

10. Read, B.J., Won, L., Kraft, J.C., Sappington, I., Aung, A., Wu, S., Bals, J., Chen, C., Lee, K.K., Lingwood, D., et al. (2022). Mannose-binding lectin and complement mediate follicular localization and enhanced immunogenicity of diverse protein nanoparticle immunogens. Cell Rep. *38*, 110217. https://doi.org/10.1016/j.celrep.2021.110217.

11. Kato, Y., Abbott, R.K., Freeman, B.L., Haupt, S., Groschel, B., Silva, M., Menis, S., Irvine, D.J., Schief, W.R., and Crotty, S. (2020). Multifaceted effects of antigen valency on B cell response composition and differentiation in vivo. Immunity *53*, 548–563.e8. https://doi.org/10.1016/j.immuni.2020.08.001.

12. Kelly, H.G., Kent, S.J., and Wheatley, A.K. (2019). Immunological basis for enhanced immunity of nanoparticle vaccines. Expert Rev. Vaccines *18*, 269–280. https://doi.org/10.1080/14760584.2019.1578216.

13. Kanekiyo, M., Wei, C.-J., Yassine, H.M., McTamney, P.M., Boyington, J.C., Whittle, J.R.R., Rao, S.S., Kong, W.-P., Wang, L., and Nabel, G.J. (2013). Self-assembling influenza nanoparticle vaccines elicit broadly

neutralizing H1N1 antibodies. Nature *499*, 102–106. https://doi.org/10.1038/nature12202.

14. Jardine, J.G., Ota, T., Sok, D., Pauthner, M., Kulp, D.W., Kalyuzhniy, O., Skog, P.D., Thinnes, T.C., Bhullar, D., Briney, B., et al. (2015). HIV-1 VACCINES. Priming a broadly neutralizing antibody response to HIV-1 using a germline-targeting immunogen. Science *349*, 156–161. https://doi.org/10.1126/science.aac5894.

15. Ingale, J., Stano, A., Guenaga, J., Sharma, S.K., Nemazee, D., Zwick, M.B., and Wyatt, R.T. (2016). High-density array of well-ordered HIV-1 spikes on synthetic liposomal nanoparticles efficiently activate B cells. Cell Rep. *15*, 1986–1999. https://doi.org/10.1016/j.celrep.2016.04.078.

16. Martinez-Murillo, P., Tran, K., Guenaga, J., Lindgren, G., Àdori, M., Feng, Y., Phad, G.E., Vázquez Bernat, N.V., Bale, S., Ingale, J., et al. (2017). Particulate array of well-ordered HIV Clade C env trimers elicits neutralizing antibodies that display a unique V2 cap approach. Immunity *46*, 804–817.e7. https://doi.org/10.1016/j.immuni.2017.04.021.

17. Brouwer, P.J.M., Antanasijevic, A., Berndsen, Z., Yasmeen, A., Fiala, B., Bijl, T.P.L., Bontjer, I., Bale, J.B., Sheffler, W., Allen, J.D., et al. (2019). Enhancing and shaping the immunogenicity of native-like HIV-1 envelope trimers with a two-component protein nanoparticle. Nat. Commun. *10*, 4272. https://doi.org/10.1038/s41467-019-12080-1.

18. Ueda, G., Antanasijevic, A., Fallas, J.A., Sheffler, W., Copps, J., Ellis, D., Hutchinson, G.B., Moyer, A., Yasmeen, A., Tsybovsky, Y., et al. (2020). Tailored design of protein nanoparticle scaffolds for multivalent presentation of viral glycoprotein antigens. eLife *9*, e57659. https://doi.org/10.7554/eLife.57659.

19. Walls, A.C., Fiala, B., Schäfer, A., Wrenn, S., Pham, M.N., Murphy, M., Tse, L.V., Shehata, L., O'Connor, M.A., Chen, C., et al. (2020). Elicitation of potent neutralizing antibody responses by designed protein nanoparticle vaccines for SARS-CoV-2. Cell *183*, 1367–1382.e17. https://doi.org/10.1016/j.cell.2020.10.043.

20. Brouwer, P.J.M., Brinkkemper, M., Maisonnasse, P., Dereuddre-Bosquet, N., Grobben, M., Claireaux, M., de Gast, M.d., Marlin, R., Chesnais, V., Diry, S., et al. (2021). Two-component spike nanoparticle vaccine protects macaques from SARS-CoV-2 infection. Cell *184*, 1188–1200.e19. https://doi.org/10.1016/j.cell.2021.01.035.

21. Boyoglu-Barnum, S., Ellis, D., Gillespie, R.A., Hutchinson, G.B., Park, Y.J., Moin, S.M., Acton, O.J., Ravichandran, R., Murphy, M., Pettie, D., et al. (2021). Quadrivalent influenza nanoparticle vaccines induce broad protection. Nature *592*, 623–628. https://doi.org/10.1038/s41586-021-03365-x.

22. Graham, B.S., Gilman, M.S.A., and McLellan, J.S. (2019). Structure-based vaccine antigen design. Annu. Rev. Med. *70*, 91–104. https://doi.org/10.1146/annurev-med-121217-094234.

23. McLellan, J.S., Chen, M., Joyce, M.G., Sastry, M., Stewart-Jones, G.B.E., Yang, Y., Zhang, B., Chen, L., Srivatsan, S., Zheng, A., et al. (2013). Structure-based design of a fusion glycoprotein vaccine for respiratory syncytial virus. Science *342*, 592–598. https://doi.org/10.1126/science.1243283.

24. Crank, M.C., Ruckwardt, T.J., Chen, M., Morabito, K.M., Phung, E., Costner, P.J., Holman, L.A., Hickman, S.P., Berkowitz, N.M., Gordon, I.J., et al. (2019). A proof of concept for structure-based vaccine design targeting RSV in humans. Science *365*, 505–509. https://doi.org/10.1126/science.aav9033.

25. Ruckwardt, T.J., Morabito, K.M., Phung, E., Crank, M.C., Costner, P.J., Holman, L.A., Chang, L.A., Hickman, S.P., Berkowitz, N.M., Gordon, I.J., et al. (2021). Safety, tolerability, and immunogenicity of the respiratory syncytial virus prefusion F subunit vaccine DS-Cav1: a phase 1, randomised, open-label, dose-escalation clinical trial. Lancet Respir. Med. *9*, 1111–1120. https://doi.org/10.1016/S2213-2600(21)00098-9.

26. Simões, E.A.F., Center, K.J., Tita, A.T.N., Swanson, K.A., Radley, D., Houghton, J., McGrory, S.B., Gomme, E., Anderson, M., Roberts, J.P., et al. (2022). Prefusion F protein–based respiratory syncytial virus immunization in pregnancy. N. Engl. J. Med. *386*, 1615–1626. https://doi.org/10.1056/NEJMoa2106062.

27. Ngwuta, J.O., Chen, M., Modjarrad, K., Joyce, M.G., Kanekiyo, M., Kumar, A., Yassine, H.M., Moin, S.M., Killikelly, A.M., Chuang, G.-Y., et al. (2015). Prefusion F–specific antibodies determine the magnitude of RSV neutralizing activity in human sera. Sci. Transl. Med. *7*, 309ra162. https://doi.org/10.1126/scitranslmed.aac4241.

28. Gilman, M.S.A., Castellanos, C.A., Chen, M., Ngwuta, J.O., Goodwin, E., Moin, S.M., Mas, V., Melero, J.A., Wright, P.F., Graham, B.S., et al. (2016). Rapid profiling of RSV antibody repertoires from the memory B cells of naturally infected adult donors. Sci. Immunol. *1*, eaaj1879. https://doi.org/10.1126/sciimmunol.aaj1879.

29. Liang, F., Lindgren, G., Sandgren, K.J., Thompson, E.A., Francica, J.R., Seubert, A., De Gregorio, E.D., Barnett, S., O'Hagan, D.T., Sullivan, N.J., et al. (2017). Vaccine priming is restricted to draining lymph nodes and controlled by adjuvant-mediated antigen uptake. Sci. Transl. Med. *9*, eaal2094. https://doi.org/10.1126/scitranslmed.aal2094.

30. Ols, S., Yang, L., Thompson, E.A., Pushparaj, P., Tran, K., Liang, F., Lin, A., Eriksson, B., Karlsson Hedestam, G.B.K., Wyatt, R.T., and Loré, K. (2020). Route of vaccine administration alters antigen trafficking but not innate or adaptive immunity. Cell Rep. *30*, 3964–3971.e7. https://doi.org/10.1016/j.celrep.2020.02.111.

31. Martin, J.T., Cottrell, C.A., Antanasijevic, A., Carnathan, D.G., Cossette, B.J., Enemuo, C.A., Gebru, E.H., Choe, Y., Viviano, F., Fischinger, S., et al. (2020). Targeting HIV Env immunogens to B cell follicles in nonhuman primates through immune complex or protein nanoparticle formulations. npj Vaccines *5*, 72. https://doi.org/10.1038/s41541-020-00223-1.

32. Martin, J.T., Hartwell, B.L., Kumarapperuma, S.C., Melo, M.B., Carnathan, D.G., Cossette, B.J., Adams, J., Gong, S., Zhang, W., Tokatlian, T., et al. (2021). Combined PET and whole-tissue imaging of lymphatic-targeting vaccines in non-human primates. Biomaterials *275*, 120868. https://doi.org/10.1016/j.biomaterials.2021.120868.

33. Cirelli, K.M., Carnathan, D.G., Nogal, B., Martin, J.T., Rodriguez, O.L., Upadhyay, A.A., Enemuo, C.A., Gebru, E.H., Choe, Y., Viviano, F., et al. (2019). Slow delivery immunization enhances HIV neutralizing antibody and germinal center responses via modulation of immunodominance. Cell *177*, 1153–1171.e1128. https://doi.org/10.1016/j.cell.2019.04.012.

34. Tam, H.H., Melo, M.B., Kang, M., Pelet, J.M., Ruda, V.M., Foley, M.H., Hu, J.K., Kumari, S., Crampton, J., Baldeon, A.D., et al. (2016). Sustained antigen availability during germinal center initiation enhances antibody responses to vaccination. Proc. Natl. Acad. Sci. USA *113*, E6639–E6648. https://doi.org/10.1073/pnas.1606050113.

35. McDonald, T.P., Jeffree, C.E., Li, P., Rixon, H.W.M., Brown, G., Aitken, J.D., MacLellan, K., and Sugrue, R.J. (2006). Evidence that maturation of the N-linked glycans of the respiratory syncytial virus (RSV) glycoproteins is required for virus-mediated cell fusion: the effect of α-mannosidase inhibitors on RSV infectivity. Virology *350*, 289–301. https://doi.org/10.1016/j.virol.2006.01.023.

36. McLellan, J.S., Chen, M., Leung, S., Graepel, K.W., Du, X., Yang, Y., Zhou, T., Baxa, U., Yasuda, E., Beaumont, T., et al. (2013). Structure of RSV fusion glycoprotein trimer bound to a prefusion-specific neutralizing antibody. Science *340*, 1113–1117. https://doi.org/10.1126/science.1234914.

37. McLellan, J.S., Yang, Y., Graham, B.S., and Kwong, P.D. (2011). Structure of respiratory syncytial virus fusion glycoprotein in the postfusion conformation reveals preservation of neutralizing epitopes. J. Virol. *85*, 7788–7796. https://doi.org/10.1128/JVI.00555-11.

38. Phung, E., Chang, L.A., Morabito, K.M., Kanekiyo, M., Chen, M., Nair, D., Kumar, A., Chen, G.L., Ledgerwood, J.E., Graham, B.S., and Ruckwardt, T.J. (2019). Epitope-specific serological assays for RSV: conformation matters. Vaccines *7*, 23. https://doi.org/10.3390/vaccines7010023.

39. Abbott, R.K., Lee, J.H., Menis, S., Skog, P., Rossi, M., Ota, T., Kulp, D.W., Bhullar, D., Kalyuzhniy, O., Havenar-Daughton, C., et al. (2018). Precursor frequency and affinity determine B cell competitive fitness in germinal centers, tested with germline-targeting HIV vaccine immunogens. Immunity *48*, 133–146.e136. https://doi.org/10.1016/j.immuni.2017.11.023.

40. Phad, G.E., Pushparaj, P., Tran, K., Dubrovskaya, V., Àdori, M., Martinez-Murillo, P., Vázquez Bernat, N.V., Singh, S., Dionne, G., O'Dell, S., et al. (2020). Extensive dissemination and intraclonal maturation of HIV Env vaccine-induced B cell responses. J. Exp. Med. *217*, e20191155. https://doi.org/10.1084/jem.20191155.

41. Corti, D., Bianchi, S., Vanzetta, F., Minola, A., Perez, L., Agatic, G., Guarino, B., Silacci, C., Marcandalli, J., Marsland, B.J., et al. (2013). Cross-neutralization of four paramyxoviruses by a human monoclonal antibody. Nature *501*, 439–443. https://doi.org/10.1038/nature12442.

42. Mousa, J.J., Binshtein, E., Human, S., Fong, R.H., Alvarado, G., Doranz, B.J., Moore, M.L., Ohi, M.D., and Crowe, J.E. (2018). Human antibody recognition of antigenic site IV on Pneumovirus fusion proteins. PLoS Pathog. *14*, e1006837. https://doi.org/10.1371/journal.ppat.1006837.

43. Xiao, X., Tang, A., Cox, K.S., Wen, Z., Callahan, C., Sullivan, N.L., Nahas, D.D., Cosmi, S., Galli, J.D., Minnier, M., et al. (2019). Characterization of potent RSV neutralizing antibodies isolated from human memory B cells and identification of diverse RSV/hMPV cross-neutralizing epitopes. mAbs *11*, 1415–1427. https://doi.org/10.1080/19420862.2019.1654304.

44. Wargacki, A.J., Wörner, T.P., van de Waterbeemd, M.v.d., Ellis, D., Heck, A.J.R., and King, N.P. (2021). Complete and cooperative in vitro assembly of computationally designed self-assembling protein nanomaterials. Nat. Commun. *12*, 883. https://doi.org/10.1038/s41467-021-21251-y.

45. Krarup, A., Truan, D., Furmanova-Hollenstein, P., Bogaert, L., Bouchier, P., Bisschop, I.J.M., Widjojoatmodjo, M.N., Zahn, R., Schuitemaker, H., McLellan, J.S., and Langedijk, J.P.M. (2015). A highly stable prefusion RSV F vaccine derived from structural analysis of the fusion mechanism. Nat. Commun. *6*, 8143. https://doi.org/10.1038/ncomms9143.

46. Swanson, K.A., Rainho-Tomko, J.N., Williams, Z.P., Lanza, L., Peredelchuk, M., Kishko, M., Pavot, V., Alamares-Sapuay, J., Adhikarla, H., Gupta, S., et al. (2020). A respiratory syncytial virus (RSV) F protein nanoparticle vaccine focuses antibody responses to a conserved neutralization domain. Sci. Immunol. *5*, eaba6466. https://doi.org/10.1126/sciimmunol.aba6466.

47. Che, Y., Gribenko, A.V., Song, X., Handke, L.D., Efferen, K.S., Tompkins, K., Kodali, S., Nunez, L., Prasad, A.K., Phelan, L.M., et al. (2023). Rational design of a highly immunogenic prefusion-stabilized F glycoprotein antigen for a respiratory syncytial virus vaccine. Sci. Transl. Med. *15*, eade6422. https://doi.org/10.1126/scitranslmed.ade6422.

48. Schwickert, T.A., Victora, G.D., Fooksman, D.R., Kamphorst, A.O., Mugnier, M.R., Gitlin, A.D., Dustin, M.L., and Nussenzweig, M.C. (2011). A dynamic T cell–limited checkpoint regulates affinity-dependent B cell entry into the germinal center. J. Exp. Med. *208*, 1243–1252. https://doi.org/10.1084/jem.20102477.

49. Shih, T.-A.Y., Meffre, E., Roederer, M., and Nussenzweig, M.C. (2002). Role of BCR affinity in T cell–dependent antibody responses in vivo. Nat. Immunol. *3*, 570–575. https://doi.org/10.1038/ni803.

50. Tas, J.M.J., Mesin, L., Pasqual, G., Targ, S., Jacobsen, J.T., Mano, Y.M., Chen, C.S., Weill, J.-C., Reynaud, C.-A., Browne, E.P., et al. (2016). Visualizing antibody affinity maturation in germinal centers. Science *351*, 1048–1054. https://doi.org/10.1126/science.aad3439.

51. Murugan, R., Buchauer, L., Triller, G., Kreschel, C., Costa, G., Pidelaserra Martí, G.P., Imkeller, K., Busse, C.E., Chakravarty, S., Sim, B.K.L., et al. (2018). Clonal selection drives protective memory B cell responses in controlled human malaria infection. Sci. Immunol. *3*, eaap8029. https://doi.org/10.1126/sciimmunol.aap8029.

52. Escolano, A., Gristick, H.B., Abernathy, M.E., Merkenschlager, J., Gautam, R., Oliveira, T.Y., Pai, J., West, A.P., Barnes, C.O., Cohen, A.A., et al. (2019). Immunization expands HIV-1 V3-glycan specific B-cells in mice and macaques. Nature *570*, 468–473. https://doi.org/10.1038/s41586-019-1250-z.

53. Walls, A.C., Miranda, M.C., Schäfer, A., Pham, M.N., Greaney, A., Arunachalam, P.S., Navarro, M.-J., Tortorici, M.A., Rogers, K., O'Connor, M.A., et al. (2021). Elicitation of broadly protective sarbecovirus immunity by receptor-binding domain nanoparticle vaccines. Cell *184*, 5432–5447.e16. https://doi.org/10.1016/j.cell.2021.09.015.

54. Cohen, A.A., Gnanapragasam, P.N.P., Lee, Y.E., Hoffman, P.R., Ou, S., Kakutani, L.M., Keeffe, J.R., Wu, H.-J., Howarth, M., West, A.P., et al. (2021). Mosaic nanoparticles elicit cross-reactive immune responses to zoonotic coronaviruses in mice. Science *371*, 735–741. https://doi.org/10.1126/science.abf6840.

55. Battles, M.B., Más, V., Olmedillas, E., Cano, O., Vázquez, M., Rodríguez, L., Melero, J.A., and McLellan, J.S. (2017). Structure and immunogenicity of pre-fusion-stabilized human Metapneumovirus F glycoprotein. Nat. Commun. *8*, 1528. https://doi.org/10.1038/s41467-017-01708-9.

56. Hsieh, C.-L., Rush, S.A., Palomo, C., Chou, C.-W., Pickens, W., Más, V., and McLellan, J.S. (2022). Structure-based design of prefusion-stabilized human Metapneumovirus fusion proteins. Nat. Commun. *13*, 1299. https://doi.org/10.1038/s41467-022-28931-3.

57. Brouwer, P.J.M., Antanasijevic, A., de Gast, M.d., Allen, J.D., Bijl, T.P.L., Yasmeen, A., Ravichandran, R., Burger, J.A., Ozorowski, G., Torres, J.L., et al. (2021). Immunofocusing and enhancing autologous Tier-2 HIV-1 neutralization by displaying Env trimers on two-component protein nanoparticles. npj Vaccines *6*, 24. https://doi.org/10.1038/s41541-021-00285-9.

58. Mousa, J.J., Kose, N., Matta, P., Gilchuk, P., and Crowe, J.E. (2017). A novel pre-fusion conformation-specific neutralizing epitope on the respiratory syncytial virus fusion protein. Nat. Microbiol. *2*, 16271. https://doi.org/10.1038/nmicrobiol.2016.271.

59. Gilman, M.S.A., Furmanova-Hollenstein, P., Pascual, G., B van 't Wout, A.B.v.t., Langedijk, J.P.M., and McLellan, J.S. (2019). Transient opening of trimeric prefusion RSV F proteins. Nat. Commun. *10*, 2105. https://doi.org/10.1038/s41467-019-09807-5.

60. Flynn, J.A., Durr, E., Swoyer, R., Cejas, P.J., Horton, M.S., Galli, J.D., Cosmi, S.A., Espeseth, A.S., Bett, A.J., and Zhang, L. (2016). Stability characterization of a vaccine antigen based on the respiratory syncytial virus fusion glycoprotein. PLoS One *11*, e0164789. https://doi.org/10.1371/journal.pone.0164789.

61. Gilman, M.S., Moin, S.M., Mas, V., Chen, M., Patel, N.K., Kramer, K., Zhu, Q., Kabeche, S.C., Kumar, A., Palomo, C., et al. (2015). Characterization of a prefusion-specific antibody that recognizes a quaternary, cleavage-dependent epitope on the RSV fusion glycoprotein. PLoS Pathog. *11*, e1005035. https://doi.org/10.1371/journal.ppat.1005035.

62. Hotard, A.L., Shaikh, F.Y., Lee, S., Yan, D., Teng, M.N., Plemper, R.K., Crowe, J.E., and Moore, M.L. (2012). A stabilized respiratory syncytial virus reverse genetics system amenable to recombination-mediated mutagenesis. Virology *434*, 129–136. https://doi.org/10.1016/j.virol.2012.09.022.

63. Bale, J.B., Gonen, S., Liu, Y., Sheffler, W., Ellis, D., Thomas, C., Cascio, D., Yeates, T.O., Gonen, T., King, N.P., and Baker, D. (2016). Accurate design of megadalton-scale two-component icosahedral protein complexes. Science *353*, 389–394. https://doi.org/10.1126/science.aaf8818.

64. Sundling, C., Li, Y., Huynh, N., Poulsen, C., Wilson, R., O'Dell, S., Feng, Y., Mascola, J.R., Wyatt, R.T., and Karlsson Hedestam, G.B.K. (2012). High-resolution definition of vaccine-elicited B cell responses against the HIV primary receptor Binding Site. Sci. Transl. Med. *4*, 142ra96. https://doi.org/10.1126/scitranslmed.3003752.

65. Sundling, C., Phad, G., Douagi, I., Navis, M., and Karlsson Hedestam, G.B. (2012). Isolation of antibody V(D)J sequences from single cell sorted rhesus macaque B cells. J. Immunol. Methods *386*, 85–93. https://doi.org/10.1016/j.jim.2012.09.003.

66. Vázquez Bernat, N., Corcoran, M., Hardt, U., Kaduk, M., Phad, G.E., Martin, M., and Karlsson Hedestam, G.B. (2019). High-quality library preparation for NGS-based immunoglobulin germline gene inference and repertoire expression analysis. Front. Immunol. *10*, 660. https://doi.org/10.3389/fimmu.2019.00660.

67. Vázquez Bernat, N., Corcoran, M., Nowak, I., Kaduk, M., Dopico, X.C., Narang, S., Maisonasse, P., Dereuddre-Bosquet, N., Murrell, B., and Hedestam, G.B.K. (2021). Rhesus and cynomolgus macaque immunoglobulin heavy-chain genotyping yields comprehensive databases of

germline VDJ alleles. Immunity *54*, 355–366.e354. https://doi.org/10.1016/j.immuni.2020.12.018.

68. Corcoran, M.M., Phad, G.E., Vázquez Bernat, N., Stahl-Hennig, C., Sumida, N., Persson, M.A., Martin, M., and Karlsson Hedestam, G.B. (2016). Production of individualized V gene databases reveals high levels of immunoglobulin genetic diversity. Nat. Commun. *7*, 13642. https://doi.org/10.1038/ncomms13642.

69. Edgar, R.C. (2004). MUSCLE: multiple sequence alignment with high accuracy and high throughput. Nucleic Acids Res. *32*, 1792–1797. https://doi.org/10.1093/nar/gkh340.

70. Price, M.N., Dehal, P.S., and Arkin, A.P. (2010). FastTree 2 – Approximately maximum-likelihood trees for large alignments. PLoS One *5*, e9490. https://doi.org/10.1371/journal.pone.0009490.

71. Kaplinsky, J., and Arnaout, R. (2016). Robust estimates of overall immune-repertoire diversity from high-throughput measurements on samples. Nat. Commun. *7*, 11881. https://doi.org/10.1038/ncomms11881.

72. Wang, L.-G., Lam, T.T.-Y., Xu, S., Dai, Z., Zhou, L., Feng, T., Guo, P., Dunn, C.W., Jones, B.R., Bradley, T., et al. (2020). treeio: an R package for phylogenetic tree input and output with richly annotated and associated data. Mol. Biol. Evol. *37*, 599–603. https://doi.org/10.1093/molbev/msz240.

73. Yu, G., Smith, D.K., Zhu, H., Guan, Y., and Lam, T.T.Y. (2017). ggtree: an R package for visualization and annotation of phylogenetic trees with their covariates and other associated data. Methods Ecol. Evol. *8*, 28–36. https://doi.org/10.1111/2041-210X.12628.

74. Suloway, C., Pulokas, J., Fellmann, D., Cheng, A., Guerra, F., Quispe, J., Stagg, S., Potter, C.S., and Carragher, B. (2005). Automated molecular microscopy: the new Leginon system. J. Struct. Biol. *151*, 41–60. https://doi.org/10.1016/j.jsb.2005.03.010.

75. Mindell, J.A., and Grigorieff, N. (2003). Accurate determination of local defocus and specimen tilt in electron microscopy. J. Struct. Biol. *142*, 334–347. https://doi.org/10.1016/s1047-8477(03)00069-8.

76. Grant, T., Rohou, A., and Grigorieff, N. (2018). cisTEM, user-friendly software for single-particle image processing. eLife *7*, e35383. https://doi.org/10.7554/eLife.35383.

77. Kimanius, D., Forsberg, B.O., Scheres, S.H.W., and Lindahl, E. (2016). Accelerated cryo-EM structure determination with parallelisation using GPUs in RELION-2. eLife *5*, e18722. https://doi.org/10.7554/eLife.18722.

78. Scheres, S.H.W. (2012). RELION: implementation of a Bayesian approach to cryo-EM structure determination. J. Struct. Biol. *180*, 519–530. https://doi.org/10.1016/j.jsb.2012.09.006.

79. Zivanov, J., Nakane, T., Forsberg, B.O., Kimanius, D., Hagen, W.J.H., Lindahl, E., and Scheres, S.H.W. (2018). New tools for automated high-resolution cryo-EM structure determination in RELION-3. eLife *7*, e42166. https://doi.org/10.7554/eLife.42166.

80. Punjani, A., Rubinstein, J.L., Fleet, D.J., and Brubaker, M.A. (2017). cryoSPARC: algorithms for rapid unsupervised cryo-EM structure determination. Nat. Methods *14*, 290–296. https://doi.org/10.1038/nmeth.4169.

81. Biacchesi, S., Skiadopoulos, M.H., Tran, K.C., Murphy, B.R., Collins, P.L., and Buchholz, U.J. (2004). Recovery of human Metapneumovirus from cDNA: optimization of growth in vitro and expression of additional genes. Virology *321*, 247–259. https://doi.org/10.1016/j.virol.2003.12.020.

82. Joyce, M.G., Zhang, B., Ou, L., Chen, M., Chuang, G.-Y., Druz, A., Kong, W.-P., Lai, Y.-T., Rundlet, E.J., Tsybovsky, Y., et al. (2016). Iterative structure-based improvement of a respiratory syncytial virus fusion glycoprotein vaccine. Nat. Struct. Mol. Biol. *23*, 811–820. https://doi.org/10.1038/nsmb.3267.

83. Spångberg, M., Martinez, P., Fredlund, H., Karlsson Hedestam, G.B., and Sundling, C. (2014). A simple and safe technique for longitudinal bone marrow aspiration in cynomolgus and rhesus macaques. J. Immunol. Methods *408*, 137–141. https://doi.org/10.1016/j.jim.2014.05.004.

84. Gasteiger, E., Hoogland, C., Gattiker, A., Duvaud, S.e., Wilkins, M.R., Appel, R.D., and Bairoch, A. (2005). The Proteomics Protocols Handbook (Springer), pp. 571–607. https://doi.org/10.1385/1-59259-890-0:571.

85. Sundling, C., Forsell, M.N., O'Dell, S., Feng, Y., Chakrabarti, B., Rao, S.S., Loré, K., Mascola, J.R., Wyatt, R.T., Douagi, I., and Hedestam, G.B. (2010). Soluble HIV-1 Env trimers in adjuvant elicit potent and diverse functional B cell responses in primates. J. Exp. Med. *207*, 2003–2017. https://doi.org/10.1084/jem.20100025.

86. Chiu, C.H., Wang, Y.T., Walther, B.A., and Chao, A. (2014). An improved nonparametric lower bound of species richness via a modified good–turing frequency formula. Biometrics *70*, 671–682. https://doi.org/10.1111/biom.12200.

87. Tavaré, S. (1986). Some probabilistic and statistical problems in the analysis of DNA sequences. Lect. Math. Life Sci. *17*, 57–86.

88. Veesler, D., Cupelli, K., Burger, M., Gräber, P., Stehle, T., and Johnson, J.E. (2014). Single-particle EM reveals plasticity of interactions between the adenovirus penton base and integrin αVβ3. Proc. Natl. Acad. Sci. USA *111*, 8815–8819. https://doi.org/10.1073/pnas.1404575111.

89. Weaver, G.C., Villar, R.F., Kanekiyo, M., Nabel, G.J., Mascola, J.R., and Lingwood, D. (2016). In vitro reconstitution of B cell receptor–antigen interactions to evaluate potential vaccine candidates. Nat. Protoc. *11*, 193–213. https://doi.org/10.1038/nprot.2016.009.

90. Corbett, K.S., Moin, S.M., Yassine, H.M., Cagigi, A., Kanekiyo, M., Boyoglu-Barnum, S., Myers, S.I., Tsybovsky, Y., Wheatley, A.K., Schramm, C.A., et al. (2019). Design of nanoparticulate Group 2 influenza virus hemagglutinin stem antigens that activate unmutated ancestor B cell receptors of broadly neutralizing antibody lineages. mBio *10*, e02810–e02818. https://doi.org/10.1128/mBio.02810-18.

STAR★METHODS

KEY RESOURCES TABLE

REAGENT or RESOURCE	SOURCE	IDENTIFIER
Antibodies		
Mouse anti-human CD1c PE (AD5-8E7)	Miltenyi	Cat#130-113-302, RRID:AB_2726081
Mouse anti-human CD11c PE-Cy7 (3.9)	Biolegend	Cat#301608, RRID:AB_389351
Mouse anti-human CD66abce FITC (TET2)	Miltenyi	Cat#130-093-132, RRID:AB_871698
Mouse anti-human CCR7 PE-Dazzle594 (G043H7)	Biolegend	Cat#353236, RRID:AB_2563641
Mouse anti-human CD3 APC-Cy7 (SP34-2)	BD Biosciences	Cat#557757, RRID:AB_396863
Mouse anti-human CD8 APC-Cy7 (RPA-T8)	BD Biosciences	Cat#557760, RRID:AB_396865
Mouse anti-human CD20 APC-Cy7 (L27)	BD Biosciences	Cat#335829, RRID:AB_2868690
Mouse anti-human CD40 BV421 (5C3)	Biolegend	Cat#334332, RRID:AB_2564211
Mouse anti-human HLA-DR PE-Cy5.5 (Tu36)	Invitrogen	Cat#MHLDR18, RRID:AB_10372966
Mouse anti-human CD14 BV570 (M5E2)	Biolegend	Cat#301832, RRID:AB_2563629
Mouse anti-human CD123 BV510 (6H6)	Biolegend	Cat#306022, RRID:AB_2562068
Mouse anti-human CD80 BV650 (L307.4)	BD Biosciences	Cat#564158, RRID:AB_2738630
Mouse anti-human CD16 AF700 (3G8)	Biolegend	Cat#302025, RRID:AB_493748
Mouse anti-NHP CD45 BV605 (D058-1283)	BD Biosciences	Cat#564098, RRID:AB_2738590
Mouse anti-His tag (AD1.1.10)	R&D Systems	Cat#MAB050, RRID:AB_357353
Polyclonal goat anti-monkey IgG antibody, HRP-conjugated	Nordic MUbio	Cat# GAMon/IgG(Fc)/PO
Polyclonal goat anti-human MBL, biotinylated	R&D Systems	Cat#BAF2307, RRID:AB_2140048
Polyclonal goat anti-human IgG (Fcγ-specific), HRP-conjugated	Jackson ImmunoResearch	Cat#109-035-008, RRID:AB_2337579
Polyclonal goat anti-human IgG (Fcγ-specific)	Jackson ImmunoResearch	Cat#109-005-008, RRID:AB_2337534
Polyclonal goat anti-human IgG (Fcγ-specific), biotinylated	Jackson ImmunoResearch	Cat#109-065-008, RRID:AB_2337623
Mouse anti-human CCR7 BV421 (G043H7)	Biolegend	Cat#353208, RRID:AB_11203894
Mouse anti-human CD4 PE-Cy5.5 (S3.5)	Invitrogen	Cat#MHCD0418, RRID:AB_10376013
Mouse anti-human CD8a BV570 (RPA-T8)	Biolegend	Cat#301038, RRID:AB_2563213
Mouse anti-human CD45RA PE-Cy5 (5H9)	BD Biosciences	Cat#552888, RRID:AB_394517
Mouse anti-human IL-21 AF647 (3A3-N2.1)	BD Biosciences	Cat#560493, RRID:AB_1645421
Rat anti-human IL-13 PE (JES10-5a2)	Biolegend	Cat#501903, RRID:AB_315198
Mouse anti-human TNF AF488 (MAb11)	Biolegend	Cat#502915, RRID:AB_493121
Rat anti-human IL-2 BV605 (MQ1-17H12)	BD Biosciences	Cat#564165, RRID:AB_2738636
Mouse anti-human IL-17A BV785 (BL168)	Biolegend	Cat#512338, RRID:AB_2566765
Mouse anti-human CD69 ECD (TP1.55.3)	Beckman Coulter	Cat#6607110, RRID:AB_1575978
Mouse anti-human IFN-gamma AF700 (B27)	Biolegend	Cat# 506516, RRID:AB_961351
Mouse anti-human CD20 BV570 (2H7)	Biolegend	Cat#302332, RRID:AB_2563805
Mouse anti-human IgG BV786 (G18-145)	BD Biosciences	Cat#564230, RRID:AB_2738684
Mouse anti-human BCL6 PE-Cy7 (K112-91)	BD Biosciences	Cat#563582, RRID:AB_2738292
Mouse anti-human Ki67 PE (B56)	BD Biosciences	Cat#556027, RRID:AB_2266296
Mouse anti-human CD3 BV510 (SP34-2)	BD Biosciences	Cat#740187, RRID:AB_2739940
Mouse anti-human CD14 BV510 (M5E2)	Biolegend	Cat#301842, RRID:AB_2561946
Mouse anti-human CD16 BV510 (3G8)	BD Biosciences	Cat#563830, RRID:AB_2938676
Mouse anti-human CD56 BV510 (B159)	BD Biosciences	Cat#740171, RRID:AB_2739924
Mouse anti-human CD19 ECD (J3-119)	Beckman Coulter	Cat#IM2708U, RRID:AB_130854
Mouse anti-human CD20 BV605 (2H7)	Biolegend	Cat#302334, RRID:AB_2563398

(Continued on next page)

Continued

REAGENT or RESOURCE	SOURCE	IDENTIFIER
Polyclonal goat anti-human IgD FITC	Southern Biotech	Cat#2030-02, RRID:AB_2795624
Mouse anti-human IgG BV786 (G18-145)	BD Biosciences	Cat#564230, RRID:AB_2738684
Mouse F(ab')₂ anti-human IgM, unlabeled	Southern Biotech	Cat#9023-01, RRID:AB_2796589
Anti-RSV-F site Ø (D25)	McLellan et al.[36]	N/A
Anti-RSV-F site I (ADI-14457)	Gilman et al.[28]	N/A
Anti-RSV-F site II (Palivizumab)	McLellan et al.[37]	N/A
Anti-RSV-F site II (Motavizumab)	McLellan et al.[37]	N/A
Anti-RSV-F site III (MPE8)	Corti et al.[41]	N/A
Anti-RSV-F site IV (101F)	McLellan et al.[37]	N/A
Anti-RSV-F site V (hRSV90)	Mousa et al.[58]	N/A
Anti-RSV-F site V (CR9501)	Gilman et al.[59]	N/A
Anti-RSV-F site I (4D7)	Flynn et al.[60]	N/A
Anti-RSV-F quaternary (AM14)	Gilman et al.[61]	N/A
Anti-RSV-F LOR antibodies	This paper	Table S1
Bacterial and virus strains		
Recombinant RSV A2 mKATE	Hotard et al.[62]	N/A
Recombinant MPV A2 GFP	ViraTree	Cat#M121
Biological samples		
Antiserum to Respiratory Syncytial Virus WHO 1ˢᵗ International Standard	NIBSC	Cat#16/284
Healthy human blood (buffy coats) from anonymous donors	Karolinska University Hospital, Stockholm, Sweden	N/A
Chemicals, peptides, and recombinant proteins		
I53-50A	Bale et al.[63]	N/A
I53-50B.4PT1	Bale et al.[63]	N/A
DS-Cav1-I53-50A	Marcandalli et al.[4]	N/A
RSV preF (DS-Cav1)	McLellan et al.[23]	N/A
RSV preF (SC-DM)	Krarup et al.[45]	N/A
RSV postF (RSV-F dFP)	McLellan et al.[37]	N/A
MPV preF (115-BV)	Battles et al.[55]	N/A
High Sensitivity NeutrAvidin-conjugated HRP	Thermo Scientific	Cat#31030
Streptavidin-conjugated APC	Biolegend	Cat#405243
Streptavidin-conjugated BV421	Biolegend	Cat#405225
Streptavidin-conjugated ALP	Mabtech	Cat#3310-10-1000
FcR Blocking Reagent, human	Miltenyi	Cat#130-059-901
1-Step Ultra TMB-ELISA Substrate Solution	Thermo Scientific	Cat#34029
BCIP/NBT substrate	Mabtech	Cat#3650-10
RSV F (DS-Cav1) overlapping peptides	This paper	N/A
Brefeldin A	Invitrogen	Cat#B7450
Staphylococcal enterotoxin B (SEB)	Sigma	Cat#S4881
CpG class B (ODN 2006)	Invivogen	Cat#tlrl-2006
Pokeweed mitogen	Sigma	Cat#L8777
Protein A from Staphylococcus aureus Cowan strain	Sigma	Cat#P7155
Liberase TL Research Grade	Sigma	Cat#5401020001
Deoxyribonuclease I (DNase I) from bovine pancreas	Sigma	Cat#DN25
Trypsin	Gibco	Cat#15090046
Sodium thiocyanate (NaSCN)	Sigma	Cat#467871

(Continued on next page)

Continued

REAGENT or RESOURCE	SOURCE	IDENTIFIER
Recombinant human mannose-binding lectin (MBL)	R&D Systems	Cat#9086-MB
Mannan from *Saccharomyces cerevisiae*	Sigma	Cat#M7504
Glycosylated I53-50 nanoparticle scaffolds	Read et al.[10]	N/A
Endopeptidase Lys-C, *Achromobacter lyticus*	Millipore Sigma	Cat#324796-2U
CaptureSelect FcXP affinity matrix	Thermo Scientific	Cat#1943712010
7-aminoactinomycin D (7-AAD)	Invitrogen	Cat#A1310
Fura Red, AM, cell permeant	ThermoFisher	Cat#F3021
SuperScript III Reverse Transcriptase	ThermoFisher	Cat#18080085
SuperScript IV Reverse Transcriptase	ThermoFisher	Cat#18090050
HotStarTaq Plus DNA Polymerase	Qiagen	Cat#203607
Critical commercial assays		
Alexa Fluor 647 NHS Ester Labeling Kit	Invitrogen	Cat#A20006
Alexa Fluor 647 Maleimide Labeling Kit	Invitrogen	Cat#A20347
LIVE/DEAD Fixable Blue viability dye	Invitrogen	Cat#L23105
Transcription Factor Buffer Set	BD Biosciences	Cat#562574
Cytofix/Cytoperm Fixation/Permeabilization Solution kit	BD Biosciences	Cat#554714
RosetteSep Human Monocyte Enrichment Cocktail	StemCell Technologies	Cat#15068
AccuCount blank beads, 8.0-12.9 μm	Spherotech	Cat#ACBP-100-10
EZ-Link™ Sulfo-NHS-LC-Biotin	Thermo Scientific	Cat#A39257
BirA biotin-protein ligase standard reaction kit	Avidity	Cat#BirA500
RNaseOUT	Invitrogen	Cat#10777019
RiboLock RNase inhibitor	Invitrogen	Cat#EO0381
RNeasy Mini Kit	Qiagen	Cat#74004
GeneJet PCR Purification Kit	Thermo Scientific	Cat#K0702
KAPA KiFi HotStart ReadyMix PCR kit	Roche	Cat#KK2601
MiniElute Gel Extraction Kit	Qiagen	Cat#28604
PCR Purification Kit	Qiagen	Cat#28004
AMPure XP Reagent for PCR Purification	Beckman Coulter	Cat#A63880
Qubit High Sensitivity dsDNA	Invitrogen	Cat#Q32851
MiSeq Reagent Kit v3, 600 cycles	Illumina	Cat#MS-102-3003
Protein A (ProA) biosensors	Sartorius	Cat#18-5010
Anti-Penta-HIS (HIS1K) biosensors	Sartorius	Cat#18-5120
Deposited data		
Raw B cell receptor sequencing reads	This paper	BioProject: PRJNA888955; https://ncbi.nlm.nih.gov/bioproject/PRJNA888955
Processed B cell receptor sequences and code	This paper	Zenodo: 7895251; https://zenodo.org/record/7895251
Experimental models: Cell lines		
Human: Expi293F Cells	ThermoFisher	Cat#A14527, RRID:CVCL_D615
Human: HEK293T Cells	ATCC	CRL-3216, RRID:CVCL_0063
Human: HEp-2 Cells	ATCC	Cat#CCL-23, RRID:CVCL_1906
Rhesus Monkey: LLC-MK2 Cells	ATCC	Cat#CCL-7, RRID:CVCL_3009
Human: RAMOS Cells	ATCC	Cat#CRL-1596, RRID:CVCL_0597
Experimental models: Organisms/strains		
Indian-origin rhesus macaques (outbred)	Astrid Fagraeus Laboratory (AFL), Stockholm, Sweden	N/A
Chinese-origin rhesus macaques (outbred)	Astrid Fagraeus Laboratory (AFL), Stockholm, Sweden	N/A

Continued

REAGENT or RESOURCE	SOURCE	IDENTIFIER
Indian-origin rhesus macaques (outbred)	Bioqual, Inc., Rockville, MD, USA	N/A
Oligonucleotides		
Primers used for RT-PCR and nested PCRs	Sundling et al.[64]; Sundling et al.[65]	N/A
Primers used for library preparation	Phad et al.[40]; Vázquez Bernat et al.[66]; Vázquez Bernat et al.[67]	N/A
Random hexamers	Invitrogen	Cat#48190011
dNTP kit	Invitrogen	Cat#10297018
Recombinant DNA		
pLVX-ZsGreen-hIgM-VH	Gift from Adrian McDermott	N/A
pLVX-mCherry-hIgM-VK	Gift from Adrian McDermott	N/A
psPAX2 plasmid	Gift from Didier Trono	Addgene plasmid # 12260, RRID:Addgene_12260
pMD2.G plasmid	Gift from Didier Trono	Addgene plasmid # 12259, RRID:Addgene_12259
Software and algorithms		
FlowJo v10	FlowJo, LLC	RRID:SCR_008520, https://www.flowjo.com/solutions/flowjo/
Prism v9	GraphPad	RRID:SCR_002798, https://www.graphpad.com/scientific-software/prism/
Illustrator v27.7	Adobe	RRID:SCR_010279, https://www.adobe.com/products/illustrator.html
ForteBio Data Analysis Software, version 12	Sartorius	https://www.sartorius.com/en/products/protein-analysis/octet-bli-detection/octet-systems-software
IgDiscover v0.15.1	Corcoran et al.[68]	https://docs.igdiscover.se/en/stable/
MUSCLE v5.1	Edgar[69]	https://www.drive5.com/muscle/
Fasttree v2.1.11	Price et al.[70]	http://www.microbesonline.org/fasttree/
R v4.2.2	CRAN	https://www.r-project.org/
scifer v0.9.3	Bioconductor	https://doi.org/10.18129/B9.bioc.scifer
vegan v2.6.4	CRAN	https://cran.r-project.org/web/packages/vegan/index.html
Recon v3.0	Kaplinsky et al.[71]	http://arnaoutlab.github.io/Recon/
treeio v1.22.0	Wang et al.[72]	https://doi.org/10.18129/B9.bioc.treeio
ggtree v.3.6.0	Yu et al.[73]	https://doi.org/10.18129/B9.bioc.ggtree
Code rendered as a webpage and raw code	This paper	https://rodrigarc.github.io/RSV-NP-repertoire/
Leginon v3.4	Suloway et al.[74]	https://emg.nysbc.org/redmine/projects/leginon/wiki/Leginon_Homepage
CTFFIND v4	Mindell and Grigorieff[75]	https://grigoriefflab.umassmed.edu/ctffind4
cisTEM v1.0.0	Grant et al.[76]	https://cistem.org/
RELION v3.1	Kimanius et al.[77]; Scheres[78]; Zivanov et al.[79]	https://github.com/3dem/relion
EPU v2	Thermo Scientific	https://www.thermofisher.com/us/en/home/electron-microscopy/products/software-em-3d-vis/epu-software.html
CryoSPARC v3.2	Punjani et al.[80]	https://cryosparc.com/download
Other		
Squalene oil-in-water emulsion (SWE) adjuvant	Vaccine Formulation Institute (VFI), Lausanne, Switzerland	N/A
Carbon Square Mesh, Cu, 400 Mesh, TH	Electron Microscopy Sciences	Cat#CF400-Cu-TH

RESOURCE AVAILABILITY

Lead contact
- Further information and requests for resources and reagents should be directed to and will be fulfilled by the lead contact, Karin Loré (karin.lore@ki.se).

Materials availability
- Antibodies generated in this study are available from the lead contact with a completed Materials Transfer Agreement (MTA).

Data and code availability
- All the sequencing data generated has been deposited at NCBI GenBank and is publicly available from the date of publication. Accession numbers are listed in the key resources table.
- Processed data and code used to perform the data analysis is available in a Zenodo repository, and also in a Github repository, and are publicly available from the date of publication. DOIs are listed in the key resources table.
- Any additional information required to reanalyze the data reported in this paper is available from the lead contact upon request.

EXPERIMENTAL MODEL AND STUDY PARTICIPANT DETAILS

Rhesus macaques
Multivalent immunogen studies
The studies were approved by the Local Ethical Committee on Animal Experiments. A total of 19 rhesus macaques (14 of Indian origin and five of Chinese origin), four females and 15 males, of four to six years of age were housed in the Astrid Fagraeus laboratory at Karolinska Institutet according to the guidelines of the Association for Assessment and Accreditation of Laboratory Animal Care. All procedures were performed abiding to the provisions and general guidelines of the Swedish Board of Agriculture. Indian-origin macaques (all males) were stratified based on age and weight into three groups (4-5 per group). Chinese-origin macaques (4 females and 1 male) made up one group of five animals.
1-mer immunogen study
Samples from 1-mer preF (DS-Cav1) and 1-mer postF immunized rhesus macaques were obtained from a previous study.[23,38] In brief, the study was approved by and conducted according to National Institutes of Health (NIH) regulations and standards on the humane care and use of laboratory animals as well as the Animal Care and Use Committees of the NIH Vaccine Research Center and Bioqual, Inc. (Rockville, Maryland). Eight male Indian-origin rhesus macaques of five to 13 years of age were housed at Bioqual, Inc. Animals were stratified based on age, weight, and sex into two groups (4 per group).
Pre-existing immunity study
The study was approved by and conducted according to National Institutes of Health (NIH) regulations and standards on the humane care and use of laboratory animals as well as the Animal Care and Use Committees of the NIH Vaccine Research Center and Bioqual, Inc. (Rockville, Maryland). Six Indian-origin rhesus macaques, two females and four males, of eight to fourteen years of age were housed at Bioqual, Inc. Animals were stratified based on age, weight, and sex into two groups (3 per group).
Immunogen tracking study
The study was approved by the Local Ethical Committee on Animal Experiments. A total of twelve rhesus macaques (five of Indian origin and seven of Chinese origin), six females and six males, of four to twelve years of age were housed in the Astrid Fagraeus laboratory at Karolinska Institutet according to the guidelines of the Association for Assessment and Accreditation of Laboratory Animal Care. All procedures were performed abiding to the provisions and general guidelines of the Swedish Board of Agriculture. To maximize data collection and minimize the use of animals for these tracking experiments, immunizations with labeled immunogens were administered in multiple limbs per animal as we have previously described.[29,30]

Human blood
The collection and use of healthy human blood samples were performed in accordance with the Helsinki declaration and approved by the regional review board of ethics in Stockholm, Sweden. Blood was collected after informed consent. The age, sex, and genetic ancestry of the donors is unknown as they come from an anonymous sample bank.

Cell lines
HEp-2 cells (ATCC: CCL-23), a carcinoma cell line established via HeLa cell contamination, were grown at 37°C and 5% CO_2 in minimum essential media (MEM) supplemented with 10% fetal calf serum (FCS) and 1% penicillin/streptomycin. LLC-MK2 cells (ATCC: CCL-7), derived from the kidney of an adult rhesus monkey (*Macaca mulatta*) of unknown sex, were grown at 37°C and 5% CO_2 in MEM supplemented with 10% fetal calf serum (FCS) and 1% penicillin/streptomycin. RAMOS cells (ATCC: CRL-1596), a B cell line that was derived from a 3-year-old, White, male patient with Burkitt's Lymphoma, were grown at 37°C and 5% CO_2 in Dulbecco's

Modified Eagle Medium (DMEM) supplemented with 10% fetal calf serum (FCS) and 1% penicillin/streptomycin. HEK293T cells (ATCC: CRL-3216), an immortalized human embryonic kidney cell line derived from a single healthy, electively terminated female fetus of unknown parentage, were grown at 37°C and 5% CO_2 in Dulbecco's Modified Eagle Medium (DMEM) supplemented with 10% fetal calf serum (FCS) and 1% penicillin/streptomycin. All cell lines were directly obtained from ATCC and were regularly tested to be negative for mycoplasma contamination.

Virus strains

Recombinant human respiratory syncytial virus (RSV) A2 mKate[62] was propagated in HEp-2 cells from plaque purified stocks. Recombinant human metapneumovirus (MPV) A2 GFP (ViraTree)[81] was propagated in LLC-MK2 cells from other working stocks.

METHOD DETAILS

Rhesus macaque immunizations
Immunizations in RSV-F naive animals

Indian-origin macaques were stratified based on age and weight into three groups (4-5 per group). One group of four received 50 μg of DS-Cav1 (1-mer) formulated in SWE adjuvant and the other two groups of five received 50 μg of DS-Cav1 on I53-50 nanoparticles (20-mer) with or without SWE adjuvant, formulated as previously described.[4] Immunizations were given by intramuscular (I.M.) injection in the right quadricep in 0.5 mL volume at weeks 0 and 4 with the addition of a third immunization for two of the groups at week 18 or week 36. The no adjuvant group received a third immunization with SWE adjuvanted 20-mer at week 10.

Chinese-origin macaques made up one group of five animals. The group received 50 μg of DS-Cav1 on I53-50 nanoparticles at 50% antigen valency (10-mer) with SWE adjuvant. Immunizations were given I.M. in the right quadricep in 0.5 mL volume at weeks 0, 4, and 14.

Samples from 1-mer preF (DS-Cav1) and 1-mer postF immunized rhesus macaques were obtained from a previous study.[23,38] Eight Indian-origin rhesus macaques were split in two groups and immunized I.M. with 50 μg of preF or postF mixed with polyIC:LC (Oncovir). Animals received three doses at weeks 0, 4, and 26. The third dose consisted of preF for both groups.

Immunizations in RSV-F-experienced animals

Six Indian-origin rhesus macaques were stratified based on age, weight, and sex into two groups (3 per group). One group received 50 μg of DS-Cav1 (1-mer) formulated in SWE adjuvant and the other 50 μg of DS-Cav1 on I53-50 nanoparticles (20-mer) in SWE adjuvant, formulated as previously described.[4] Immunizations were given I.M. in the right quadricep in 0.5 mL volume at week 0. The animals had 4-5 years prior received immunizations with DS-Cav1 or single-chain variants of other preF constructs.[82]

Immunogenicity immunizations and sample collection

The animals were lightly sedated with ketamine at 10-15 mg/kg given intramuscularly (Ketaminol 100 mg/ml, Intervet, Sweden) during the immunizations, blood draws, and bone marrow aspirations. Bone marrow was sampled from the humerus as previously described.[83] Blood and bone marrow samples were drawn into EDTA containing vacutainer tubes. Mononuclear cells from peripheral blood (PBMCs) and bone marrow were obtained by standard density gradient centrifugation using Ficoll-Paque (Cytiva).

Animals immunized with the 20-mer and 1-mer were euthanized two weeks after receiving a third dose (i.e., boost 2). All tissues were sampled during necropsy and stored separately in RPMI1640 on ice. LNs were mechanically disrupted using a syringe plunger and 70 μm cell strainers. All individual LNs per LN cluster (axillary, apical, inguinal, external/common iliac, mesenteric, mediastinal, popliteal) were pooled for analysis. Single cell suspensions were washed and used immediately for ELISpot or flow cytometry analyses.

Tracking immunizations and terminal sample collection

To analyze the early innate immune responses and track the fate of the DS-Cav1 immunogen formulations after immunization, fluorescently labeled immunogens in SWE adjuvant were administered to twelve macaques. Animals received four I.M. injections of either Alexa Fluor 647-labeled DS-Cav1 or Alexa Fluor 647-labeled DS-Cav1-I53-50 (50 μg DS-Cav1 per injection site) formulated with 50% volume SWE adjuvant at different sites. For these experiments, I.M. administration of one labeled immunogen was performed in one deltoid and one quadricep while the other labeled immunogen was given in the contralateral deltoid and quadricep in the same animal for comparison. Phosphate-buffered saline (PBS) was administered I.M. to the calves as internal controls. This way six data points were collected from each animal. The final injection volumes were 0.5 ml and were administered on a marked injection site. Animals were immunized either two hours, 24 hours, 72 hours, or seven days prior to termination.

Protein Expression and Purification

His-tagged trimeric I53-50A and pentameric I53-50B.4PT1 proteins[63] were expressed in Lemo21(DE3) cells (NEB) in LB (10 g Tryptone, 5 g Yeast Extract, 10 g NaCl) grown in 2 L baffled shake flasks or a 10 L BioFlo 320 Fermenter (Eppendorf). Cells were grown at 37°C to an OD600 of 0.8, and then induced with 1 mM IPTG. Expression temperature was reduced to 18°C and the cells shaken for 16 h. The cells were harvested and lysed by microfluidization using a Microfluidics M110P at 18,000 psi in 50 mM Tris, 500 mM NaCl, 30 mM imidazole, 1 mM PMSF, 0.75% CHAPS. Lysates were clarified by centrifugation at 24,000 g for 30 min and applied to a 2.6× 15 cm Ni Sepharose 6 FF column (Cytiva) for purification by IMAC on an AKTA Avant150 FPLC system (Cytiva). Protein of interest was eluted over a linear gradient of 30–500 mM imidazole in a background of 50 mM Tris pH 8, 500 mM NaCl, 0.75% CHAPS buffer. Peak fractions were pooled, concentrated in 10K MWCO centrifugal filters (Millipore), sterile filtered (0.22 μm) and applied to either a

Superdex 200 Increase 10/300, or HiLoad S200 pg GL SEC column (Cytiva) using 50 mM Tris pH 8, 500 mM NaCl, 0.75% CHAPS buffer. I53-50A elutes at 0.6 column volumes (CV), while I53-50B.4PT1 elutes at 0.45 CV.

DS-Cav1-I53-50A trimer was produced as described previously.[4] DS-Cav1 soluble trimer (RSV preF),[23] SC-DM soluble trimer (RSV preF),[45] RSV-F dFP soluble trimer (RSV postF),[37] and 115-BV soluble trimer (MPV preF)[55] were produced in Expi293F cells grown in suspension using Expi293F expression medium (Life Technologies) at 33°C, 70% humidity, 8% CO_2 rotating at 150 rpm. The cultures were transiently co-transfected with furin at a 9:1 ratio using PEI-MAX (Polyscience) with cells grown to a density of 3.0 million viable cells per mL and cultivated for 3 days. Supernatants were clarified by centrifugation (5 min at 4000 rcf), addition of PDADMAC solution to a final concentration of 0.0375% (Sigma Aldrich, #409014), and a second centrifugation for 5 min at 4000 rcf. Each clarified supernatant was supplemented with 1 M Tris-HCl pH 8.0 to a final concentration of 50 mM and 5 M NaCl to a final concentration of 350 mM. The clarified, salt-treated supernatant was then incubated with 10 mL Talon resin for 10 minutes. Resin was isolated via filtration through a 0.45 μm filter, washed with 10 CV of 20 mM Tris pH 8, 300 mM NaCl, and loaded onto a 25 mL chromatography column. The flow-through was again incubated with 5 mL Talon resin in the same manner. Protein was eluted in one step with 3 CV of 25 mM Tris pH 8, 250 mM NaCl, 300 mM imidazole, 50 mM glycine, 5% v/v glycerol. The trimeric proteins were further purified using a Superdex 200 Increase 10/300 column (Cytiva) as described above.

In Vitro *Assembly of DS-Cav1-I53-50 and I53-50*

Total protein concentration of independently purified nanoparticle components was determined by measuring absorbance at 280 nm using an Agilent Cary 8454 UV/vis spectrophotometer and calculated extinction coefficients.[84] In vitro assembly of the nanoparticles was performed at room temperature with addition of the components in the following order: DS-Cav1-I53-50A trimeric fusion protein, followed by additional buffer as needed to achieve desired final concentration, and finally I53-50B.4PT1 pentameric component (in 50 mM Tris pH 8, 500 mM NaCl, 0.75% w/v CHAPS), with a molar ratio of DS-Cav1-I53-50A:I53-50B.4PT1 of 1.1:1 (subunit:subunit). To produce partial valency DS-Cav1-I53-50 nanoparticles, mixtures of DS-Cav1-I53-50A and unmodified I53-50A trimers (in 50 mM Tris pH 8, 500 mM NaCl, 0.75% w/v CHAPS) at the desired ratios were added in a slight molar excess (1.1×) to I53-50B.4PT1. All DS-Cav1-I53-50 in vitro assemblies were incubated at 2–8°C with gentle rocking for at least 30 min before subsequent purification by SEC to remove residual unassembled component using a Superose 6 Increase 10/300 GL column. Assembled particles elute at ~10 mL on the Superose 6 column. Assembled nanoparticles were sterile filtered (0.22 μm) immediately prior to column application and again following pooling of fractions.

Fluorescent Labeling of Nanoparticle Component

An antigen-free version of I53-50A trimeric component with a single cysteine (cysmut-I53-50A.1PT1) in 50 mM Tris pH 7.5, 150 mM NaCl buffer at 95.5 μM was added to an amber tube (for a total of 4.3 mg). 1 mg of Alexa Fluor 647 maleimide-conjugated fluorophore dissolved in DMSO was added dropwise to the tube and mixed thoroughly by pipetting and gentle inversion. The reaction was incubated with rocking overnight at 4°C prior to quenching with 5 mM DTT and purification by desalting on a PD10 gravity column (Cytiva), following manufacturer's instructions. The conjugated sample, referred to here as AF647-cysmut, was further purified in a polishing step by size exclusion chromatography (SEC) on an AKTA FPLC system (Cytiva) using a Superdex 200 Increase 10/300 GL column (Cytiva) TBS as the running buffer. The mg/mL concentration of AF647-cysmut was quantified by UV-Vis and corrected for fluorophore absorbance at 280 nm. Labeling efficiency was calculated to be ~15% by absorbance at 651 nm.

In Vitro *Assembly of Fluorescently Labeled DS-Cav1-I53-50*

Assembly reactions were set up such that 20% of the total trimeric components incorporated into the nanoparticle were AF647-cysmut and the remaining 80% DS-Cav1-I53-50A. Briefly, AF647-cysmut (to 10 μM) and DS-Cav1-I53-50A (to 40 μM) were added to a tube and mixed thoroughly by pipetting. Then buffer (25 mM Tris pH 8, 250 mM NaCl, 5% glycerol) was added such that the final volume of the assembly reaction was 1 mL. Finally, the I53-50B pentameric component (to 50 μM) was added to drive nanoparticle assembly. The reaction was incubated for ~1 hour prior to purification by SEC on an AKTA FPLC (Cytiva) using a Superose 6 10/300 GL column (Cytiva) and 25 mM Tris pH 8.0, 250 mM NaCl, 5% glycerol as the running buffer.

Fluorescent Labeling of DS-Cav1

DS-Cav1 protein was labeled using the Alexa Fluor 647 NHS Ester labeling kit according to the manufacturer's instructions.

ELISA assays
Antibody binding analyses

In brief, high-binding, half-area 96-well ELISA plates (Corning) were coated with either 50 μl of 2 μg/ml of DS-Cav1, PostF, MPV-F, bare I53-50 nanoparticle, or foldon protein in PBS overnight at 4°C. For bare I53-50 nanoparticle, all buffers were switched to TBS instead of PBS. The following day, plates were washed three times with PBS supplemented with 0.05% Tween-20 (PBS-T) and incubated with PBS containing 5% non-fat milk (w/v; blocking buffer) for one hour at room temperature (RT) to block unspecific binding. Plasma samples were diluted 4-fold from a starting dilution of 1:20 or 1:50 in blocking buffer. Pooled plasma samples from unimmunized and immunized animals were used as negative and positive controls, respectively, in all assays. To address the contribution of preF or postF-specific antibodies, soluble preF or postF protein was added in blocking buffer to a final concentration of 10 μg/ml and incubated for 30 min with plasma dilutions prior to addition to ELISA plates. After removal of the blocking buffer from the plates, the diluted samples were added and incubated for two hours at RT. The plates were washed three times with PBS-T before adding horseradish peroxidase (HRP)-conjugated polyclonal goat anti-monkey IgG (NordicMUbio) at 1:20,000 dilution in blocking buffer, followed by one hour incubation at RT. The plates were washed three times with PBS-T and 50 μl of 1-Step Ultra TMB-ELISA Substrate Solution (ThermoFisher) was added. After five minutes, the reaction was stopped by adding equal volume of 1M sulfuric acid. The plates

were read for absorbance at 450 nm and 570 nm on a Varioskan LUX Multimode Microplate Reader (ThermoFisher). Extinction at 570 nm was subtracted as background. The effective concentration or dilution to elicit 50% of the maximal extinction (EC50 or ED50) for each sample was determined using a four-parameter non-linear regression curve fit in GraphPad Prism version 9 (GraphPad Software Inc.).

For recombinant LOR antibodies, 4-fold serial dilutions started at 10 μg/ml and were prepared in blocking buffer in duplicates. The antibodies Palivizumab, D25, and MPE8 served as controls in all assays. Bound antibodies were detected with HRP-conjugated polyclonal goat anti-human IgG (Jackson Immunoresearch) at 1:5,000 dilution in blocking buffer.

PreF-specific IgG avidity was measured using a chaotropic wash ELISA as previously described,[30] with some modifications. Plates were coated as described above. Plasma was normalized to an OD value of 1. After sample incubation, plates were incubated with a serial dilution of sodium thiocyanate (NaSCN: 5.5, 4.5, 3.5, 2.5, 1, 0 M) diluted in PBS for 10 min. The plates were then washed and developed as described above. The avidity of the plasma IgG is reported as IC20, which is the molar concentration of NaSCN needed to dissociate 20% of the plasma binding and was calculated with a linear regression. The arithmetic mean of three independent experiments is reported.

ELISA competition analyses (epitope binning)

Epitope binning analyses were performed by ELISA competition with reference RSV-F-specific antibodies in a similar manner to as previously described.[38] The reference antibodies used were biotinylated and optimal concentrations were determined for each antibody separately. Reference antibodies included D25 (site Ø),[36] ADI-14457 (site I),[28] Palivizumab (site II),[37] MPE8 (site III),[41] 101F (site IV),[37] hRSV90 (site V),[58] and CR9501 (site V).[59] In brief, high-binding, half-area 96-well ELISA plates (Corning) were coated with 50 μl of either DS-Cav1 at 2 μg/ml or PostF at 0.5 μg/ml in PBS and incubated overnight at 4°C. The following day, plates were washed three times with PBS-T and incubated with blocking buffer for one hour at RT. Starting from 1:25 dilution or 20 μg/ml, 3-fold serial dilutions of the plasma or antibody samples were prepared in duplicates in blocking buffer and 25 μl was added to the ELISA plates. After 30 minutes of incubation at RT, 25 μl of the biotinylated reference antibody diluted in blocking buffer was added to the samples in the ELISA plates. Following an additional 90 minutes of incubation at RT, plates were washed three times with PBS-T before addition of HRP-conjugated NeutrAvidin (ThermoFisher) at 1:20,000 dilution in PBS-T. Following one hour of incubation, plates were washed three times with PBS-T and the signal was developed by adding 50 μl of 1-Step Ultra TMB-ELISA substrate solution (ThermoFisher). The reaction was stopped by adding 50 μl 1M sulfuric acid after five minutes of substrate incubation at RT. The plates were then read for absorbance at 450 nm and 570 nm on a Varioskan LUX Multimode Microplate Reader (ThermoFisher). Extinction at 570 nm was subtracted as background. For plasma samples, the effective dilution to compete 50% of the reference antibody binding (50% competing titer) for each sample was determined using a four-parameter non-linear regression curve fit in GraphPad Prism version 9 (GraphPad Software Inc.). For recombinant LOR antibodies, the area under the curve (AUC) was determined for each sample using Prism version 9 (GraphPad Software Inc.) and was then subtracted from the AUC of a non-binding antibody to determine the delta AUC (dAUC). The ratio of dAUC of each tested antibody compared to the dAUC of the reference antibody competing against itself was used to normalize values for plotting.

MBL binding ELISA

An ELISA was modified and optimized to assess the binding of mannose-binding lectin (MBL) to immunogens from methods previously described.[7] Immunogens were coated in 50 μl as duplicates on high-binding, half-area 96-well ELISA plates (Corning) as three points of a 3-fold serial dilution starting at 3 μg/ml of antigen in TBS and incubated overnight at 4°C. After coating, plates were washed three times with TBS-T-Ca (TBS containing 0.05% Tween20 and 0.1 M CaCl$_2$) and blocked for two hours at RT in blocking buffer (TBS containing 5% milk and 0.1 M CaCl$_2$). Following blocking, the wells were washed and then incubated with 50 μL of 5 μg/ml recombinant human MBL (R&D Systems) in blocking buffer for two hours at 37°C. After washing, biotinylated polyclonal goat anti-human MBL antibody (R&D Systems) was added at a 1:500 dilution in blocking buffer and incubated for two hours at 37°C. Plates were washed three times with TBS-T-Ca before addition of HRP-conjugated NeutrAvidin (ThermoFisher) at 1:10,000 dilution in TBS-T-Ca. Following one hour of incubation, plates were washed three times and the signal was developed by adding 50 μl of 1-Step Ultra TMB-ELISA substrate solution (ThermoFisher). The reaction was stopped by adding 50 μl of 1M sulfuric acid after five minutes of substrate incubation. The plates were read for absorbance at 450 nm and 570 nm on a Varioskan LUX Multimode Microplate Reader (ThermoFisher). Extinction at 570 nm was subtracted as background. The absorbance values were plotted for each three-point dilution of sample using Prism version 9 (GraphPad Software Inc.). Multiple positive and negative controls were used in the assay, including mannan from *Saccharomyces cerevisiae* (Sigma) and differentially glycosylated I53-50 scaffolds described previously.[10]

Sandwich ELISA (co-display conformation analysis)

Sandwich ELISAs were performed to confirm co-display of postF and preF on the assembled multivalent nanoparticles. High-binding, half-area 96-well ELISA plates (Corning) were coated with either 50 μl of 0.5 μg/ml D25 antibody,[36] 0.5 μg/ml Palivizumab antibody,[37] or 1 μg/ml 4D7 antibody[60] in PBS overnight at 4°C. The following day, plates were washed three times with PBS-T and incubated with blocking buffer for one hour at RT. Four-fold serial dilutions were prepared in duplicates starting from 5 μg/ml DS-Cav1, postF, SC-DM, or equimolar concentrations of the 20-mer and 10-mer nanoparticles as well as the non-assembled DS-Cav1-I53-50A nanoparticle component. Diluted samples were added to ELISA plates and incubated for one hour at RT. The plates were washed three times with PBS-T, biotinylated antibodies 4D7 (postF-specific), D25 (preF-specific), or Palivizumab (preF/postF-specific) were added and incubated for two hours at RT. Following three washes with PBS-T, the signal was developed by adding 50 μl of 1-Step Ultra TMB-ELISA substrate solution (ThermoFisher). After five minutes, the reaction was stopped by adding an equal volume of 1M sulfuric acid. The plates were read for absorbance at 450 nm and 570 nm on a Varioskan LUX Multimode Microplate

Reader (ThermoFisher). Extinction at 570 nm was subtracted as background. The AUC was determined using Prism version 9 (GraphPad software Inc.).

Virus assays

Generation of RSV working virus stock

Working stocks of recombinant RSV A2 mKate[62] were propagated from master stocks generated by four rounds of plaque purification in HEp-2 cells. Master stock virus was used to inoculate 80% confluent T175 flasks of HEp-2 cells. Diluted master stock virus was added to washed cells, incubated for 1 hour at RT with gentle rocking, then topped up to 50 mL of MEM supplemented with 10% fetal calf serum (FCS) and 1% penicillin/streptomycin, and cultured for 4 days at 37°C and 5% CO_2. Working stock was harvested by scraping cells from flasks and transferring all culture material to chilled conical tubes for sonication on ice. Cell debris was removed by centrifugation at 4°C and supernatants were aliquoted, frozen in an alcohol-dry ice slurry, and stored at -80°C. Working stocks were titrated by fluorescence in the 384-well plate format described below to achieve a signal-to-noise ratio of ∼4 at 26 hours.

RSV neutralization analyses

HEp-2 cells (ATCC: CCL-23) were diluted in culture medium (MEM or FluoroBrite DMEM with 10% FCS) to a working concentration of 0.2×10^6 cells/ml. The cells were seeded in black 384-well optically clear bottom plates (ThermoFisher Scientific) at a density of 6×10^3 cells per well and incubated overnight at 37°C and 5% CO_2. Serial 3-fold dilutions in culture media were performed on antibody samples in 96-well plates. A starting dilution of 1:10 was used for plasma or serum samples and a starting concentration of 10-30 μg/ml was used for recombinant antibodies. Recombinant RSV A2 mKate[62] was diluted 1:4-8 in culture media (depending on virus stock). Equal volumes of virus dilution were added to sample dilutions. The sample-virus mixture was briefly vortexed at low speed to mix and incubated at 37°C for one hour. Afterwards, 50 μl of the sample-virus mixture was added column-wise to the HEp-2 cells seeded the day before in 384-well plates and incubated at 37°C and 5% CO_2. Fluorescence endpoints were recorded at 26 hours using excitation at 588 nm and emission at 635 nm with bottom reading on a Varioskan LUX Multimode Microplate Reader (ThermoFisher). To address the contribution of preF- or postF-specific antibodies, soluble preF or postF protein was added to a final concentration of 20 μg/ml and incubated for 30 min with serum dilutions prior to addition of virus. The data was normalized using Prism version 9 (GraphPad Software Inc.), choosing maximum signal achieved in virus only wells as 100% infection and a fluorescence signal of 0.3 as 0% infection. The IC50 titer, which corresponds to the titer leading to 50% inhibition of infection, was calculated for each sample using a four-parameter non-linear regression curve fit.

The Antiserum to Respiratory Syncytial Virus WHO 1st International Standard 16/284 (NIBSC) was used an internal control and to normalize values of plasma or serum neutralization runs. International units were assigned to each sample using the equation IU/ml = GMT of sample / (GMT RSV International Standard / 2,000 IU/ml). EDTA plasma was verified to have no effect on the robustness of the assay.

Generation of MPV working virus stock

Working stocks of recombinant MPV A2 GFP (ViraTree)[81] were propagated from other working stocks by inoculation of 80% confluent T175 flasks of LLC-MK2 cells. Cells were washed twice with PBS, diluted virus was added to washed cells, incubated for 1 hour at RT with gentle rocking, then topped up to 16 mL of MEM supplemented with 1% penicillin/streptomycin and 5 μg/mL trypsin (i.e., no FCS), and cultured for 4-5 days at 37°C and 5% CO_2. Working stock was harvested by aspirating and discarding media, scraping cells from flasks and resuspending cells with 5 mL of cold 25% (w/v) sterile-filtered sucrose PBS solution before transferring to chilled conical tubes for sonication on ice. Cell debris was removed by centrifugation at 4°C and supernatants were aliquoted, frozen in an alcohol-dry ice slurry, and stored at -80°C. Working stocks were titrated by fluorescence in the 384-well plate format described below to achieve a signal-to-noise ratio of >6 at 48 hours.

MPV neutralization analyses

LLC-MK2 cells (ATCC: CCL-7) were diluted in culture medium (FluoroBrite DMEM with 0% FCS) to a working concentration of 0.2×10^6 cells/ml. Cells were seeded in black 384-well optically clear bottom plates (Thermo Fisher Scientific) at a density of 6×10^3 cells per well and incubated overnight at 37°C and 5% CO_2. Serial 3-fold dilutions in culture media were performed on samples in 96-well plates. A starting dilution of 1:50 was used for plasma or serum samples and a starting concentration of 10-30 μg/ml was used for recombinant antibodies. Recombinant MPV A2 GFP (ViraTree)[81] was diluted 1:8 in culture media and equal volumes of virus dilution were added to sample dilutions. The sample-virus mixture was briefly vortexed at low speed to mix and incubated at 37°C for one hour. Afterwards, 50 μl of the sample-virus mixture was added column-wise to the LLC-MK2 cells seeded the day before in 384-well plates and incubated at 37°C and 5% CO_2. Fluorescence endpoints were recorded at 48 hours using excitation at 489 nm and emission at 511 nm with bottom reading on a Varioskan LUX Multimode Microplate Reader (ThermoFisher). The data was normalized using Prism version 9 (GraphPad Software Inc.), choosing maximum signal achieved in virus only wells as 100% infection and a fluorescence signal of 0.1 as 0% infection. The IC50 titer, which corresponds to the titer leading to 50% inhibition of infection, was calculated for each sample using a four-parameter non-linear regression curve fit.

B cell ELISpot analyses

To enumerate antigen-specific plasma cells in bone marrow and memory B cells in blood enzyme-linked immunospot (ELISpot) assays were performed as previously described.[30,85] ELISpot plates (MAIPSWU10; Millipore) were coated with 10 μg/ml of goat anti-human IgG (Fcγ; Jackson ImmunoResearch). Dilution series of cells were transferred in duplicate and cultured overnight in R10 at 37°C. For bone marrow plasma cell enumeration, cells were plated directly without prior stimulation. For quantification of memory

B cells in blood, cells were first stimulated for four days at 2 million cells/ml in R10 supplemented with 5 μg/ml CpG-B (ODN 2006; Invivogen), 10 μg/ml Pokeweed mitogen (PWM; Sigma-Aldrich), and 1:10,000 Protein A from Staphylococcus aureus Cowan strain (SAC; Sigma-Aldrich). ELISpot plates were washed with PBS-T, incubated with 0.25 μg/ml biotinylated goat anti-human IgG (Fcγ; Jackson ImmunoResearch Laboratories) for total IgG determination, 1 μg/ml biotinylated DS-Cav1 trimer for preF-specific determination, or 1 μg/ml biotinylated ovalbumin (OVA) in PBS-T. After another round of washing, streptavidin-conjugated alkaline phosphatase (Mabtech) diluted in PBS-T was added. BCIP/NBT substrate (Mabtech) was used to develop spots and counts were acquired with an AID ELISpot reader (Autoimmun Diagnostika). Spots were background-subtracted using counts from OVA wells.

Flow cytometry and cell sorting
T cell antigen recall analyses
To assess F-specific T cell responses from the immunogenicity study, PBMCs were cultured overnight at 1 million cells/well in 96-well plates in R10 alone (unstimulated) or 1 μg/ml overlapping peptides (15-mers overlapping by 10 of DS-Cav1 sequence). As a positive control, 1 μg/ml of Staphylococcal enterotoxin B (SEB, Sigma) was used with at least one sample per run. After 2 hours of stimulation at 37°C, 10 μg/ml Brefeldin A (BFA; Invitrogen) was added to the cultures. After overnight culture at 37°C, cells were washed with PBS and stained with live/dead fixable blue viability dye (Invitrogen), anti-human CCR7 BV421 (G043H7, Biolegend), CD4 PE-Cy5.5 (S3.5, Invitrogen), CD8 BV570 (RPA-T8, Biolegend), and CD45RA PE-Cy5 (5H9, BD Biosciences). Cells were permeabilized using the Cytofix/Cytoperm kit (BD Biosciences) and stained intracellularly for anti-human IL-21 AF647 (3A3-N2.1, BD Biosciences), IL-13 PE (JES10-5a2, Biolegend), TNF AF488 (MAb11, Biolegend), IL-2 BV605 (MQ1-17H12, BD Biosciences), IL-17A BV785 (BL168, Biolegend), CD69 ECD (TP1.55.3, Beckman Coulter), CD3 APC-Cy7 (SP34-2, BD Biosciences), and IFNg AF700 (B27, Biolegend). Cells were washed after staining and fixed with 1% PFA before acquisition on an LSRFortessa flow cytometer (BD Biosciences). Analysis was done using FlowJo v10 (FlowJo Inc.) and results were background subtracted using values from unstimulated cells. Results are plotted from total memory CD4 T cells falling into gates Lymphocytes/Singlets/Live/CD3+/CD4+ CD8-/CCR7- CD45RA+ and CCR7- CD45RA- and CCR7+ CD45RA-.

Flow cytometry of tracking experiments
Cell suspensions from approximately 2 grams of muscle tissue or 5 million LN cells were stained for flow cytometry analysis. Briefly, Live/Dead fixable blue viability dye (Invitrogen) was used according to manufacturer's protocol, FcR-blocking reagent (Miltenyi Biotec) was used, and a cocktail of fluorescent antibodies was added. The cocktail included anti-human CD1c PE (AD5-8E7, Miltenyi), CD11c PE-Cy7 (3.9, Biolegend), CD66abce FITC (TET2, Miltenyi), CCR7 PE-Dazzle594 (G043H7, Biolegend), CD3 APC-Cy7 (SP34-2, BD Biosciences), CD8 APC-Cy7 (RPA-T8, BD Biosciences), CD20 APC-Cy7 (L27, BD Biosciences), CD40 BV421 (5C3, Biolegend), HLA-DR PE-Cy5.5 (Tu36, Invitrogen), CD14 BV570 (M5E2, Biolegend), CD123 BV510 (6H6, Biolegend), CD80 BV650 (L307.4, BD Biosciences), CD16 AF700 (3G8, Biolegend), and anti-NHP CD45 BV605 (D058-1283, BD Biosciences). Samples were spiked with AccuCount beads (Spherotech) and cell numbers were calculated according to the manufacturer's protocol. Cells were washed after staining and fixed with 1% PFA before acquisition. At least 1 million events per sample were acquired on an LSRFortessa flow cytometer (BD) and data was analyzed using FlowJo v10 (FlowJo Inc). Gating for immune cell populations was performed as shown (Figure S2A) and previously described.[30]

In vitro vaccine experiments
Buffy coats from human blood donors were used to isolate human monocytes with a Rosettesep human monocyte enrichment kit (STEMCELL Technologies) followed by standard density centrifugation. Isolated cells were used for molarity experiments with AF647-labeled immunogens by incubation of 0.5 million cells with 68 nM, 6.8 nM, 4 nM, or 0.4 nM of DS-Cav1-AF647 (1-mer-AF647) and 4 nM or 0.4 nM of DS-Cav1-I53-50-AF647 (16-mer-AF647) in R10 media for 1 hour at 37°C. After culture, cells were washed with PBS and stained with live/dead fixable blue viability dye (Invitrogen), FcR blocking reagent (Miltenyi Biotec), anti-human HLA-DR PE-Cy5.5 (Tu36, Life Technologies) and CD14 BV570 (M5E2, Biolegend). Cells were washed after staining and fixed with 1% PFA before acquisition on an LSRFortessa flow cytometer (BD Biosciences). Analysis was done using FlowJo v10 (FlowJo Inc.).

Antigen-specific GC B cell probing by flow cytometry
To assess F-specific GC B cell responses, fresh LN cell suspensions were stained with live/dead fixable blue viability dye (Invitrogen) followed by 50 ng of DS-Cav1 tetramer probes in BV421 for 30 min at 4°C. Cells were subsequently stained with anti-human CD20 BV570 (2H7, Biolegend), and CD3 APC-Cy7 (SP34-2, BD Biosciences) for an additional 20 min at 4°C. Cells were permeabilized using the transcription factor buffer set (BD Biosciences) and stained intracellularly for anti-human IgG BV786 (G18-145, BD Biosciences), BCL6 PE-Cy7 (K112-91, BD Biosciences), and Ki67 PE (B56, BD Biosciences). Tetramer DS-Cav1 probes were prepared by incubation of 4-fold molar excess of Avi-tag biotinylated DS-Cav1 protein with streptavidin-conjugated BV421 (Biolegend).

Antigen-specific memory B cell sorting
Cryopreserved PBMCs collected two weeks after the third immunization (i.e., boost 2) were thawed at 37°C and washed twice with warm R10. Cells were stained with 100 ng of fluorescent PreF-APC and PostF-BV421 probes in 100 μl R10 for 20 min at 4°C. Following a wash with R10, cells were stained with a panel of antibodies to identify memory B cells in a total volume of 100 μl R10 for 30 minutes at room temperature. The panel contained anti-human CD3 BV510 (SP34-2, BD Biosciences), CD14 BV510 (M5E2, Biolegend), CD16 BV510 (3G8, BD Biosciences), CD56 BV510 (B159, BD Biosciences), CD19 ECD (J3-119, Beckman Coulter), CD20 BV605 (2H7, Biolegend), IgD FITC (polyclonal, Southern Biotech), and IgG BV786 (G18-145,

BD Biosciences). After another wash with R10, cells were resuspended in approximately 1 ml R10 with 7aminoactinomycin D (7-AAD; Invitrogen) at a dilution of 1:4,000 and kept on ice before acquisition on a BD Aria III Fusion cell sorter. RSV-F-specific memory B cells (Lymphocytes/Singlets/Live/CD3- CD14- CD16- CD56-/CD20+ CD19+/IgD- IgG+/PreF+ PostF- and PreF+ PostF+ and PreF- PostF+; see also Figure S4A) were index-sorted into 96-well plates, immediately placed on dry ice and frozen at -80°C. Tetramer preF (DS-Cav1) and postF probes were prepared by incubation of 4-fold molar excess of Avi-tag biotinylated protein with streptavidin-conjugated BV421 (Biolegend) or streptavidin-conjugated APC (Biolegend).

BCR sequencing
Single BCR amplification and sequencing
cDNA was retrieved in one step by single cell mRNA reverse transcription. Reverse transcription mix containing 5 μl 5× First Strand buffer (Invitrogen), 4.81 mM DTT (Invitrogen), 0.77 mM dNTPs (Invitrogen), 0.24 % IGEPAL CA-630 (Sigma-Aldrich), 150 ng random hexamers (Invitrogen), 20 U RNaseOUT (Invitrogen), 100 U SuperScript III Reverse Transcriptase (Invitrogen) and nuclease-free water in a total volume of 26 μl was added to single sorted cells. Reverse transcription was performed by initial 10 min incubation at 42°C, 10 min at 25°C, 60 min at 50°C, 5 min at 94°C and final cooling to 4°C. The plates with cDNA were stored at -80°C.

Variable regions from antibody heavy, lambda, and kappa chains were amplified by nested PCR protocols adapted from Sundling et al.,[64,65] where forward and reverse primers anneal to the leader sequence and constant region, respectively, enabling amplification of the whole VDJ segment. Briefly, 1st PCR master mix contained 2.6 μl 10× Hot Star PCR buffer (Qiagen) with 15 mM MgCl$_2$, 0.25 mM dNTPs, 1.50 mM MgCl$_2$ (Qiagen), 0.10 μM 5'-primer mix (primers were supplied at 200 μM each and mixed at equal volumes), 0.10 μM 3'-primer and 1.3 U HotStarTaq Plus DNA polymerase (Qiagen). The master mix was filled to 23.7 μl with nuclease-free water and added 2.3 μl of the template cDNA. The 2nd PCR master mix consisted of 2.6 μl 10× Hot Star PCR buffer, 0.25 mM dNTPs, 5.2 μl 5× Q-solution (Qiagen), 0.63 μM 5'-primer mix (primers ware supplied at 200 μM each and mixed at equal volumes), 0.63 μM 3'-primer and 1.3 U HotStarTaq Plus DNA polymerase. Nuclease-free water was filled to 23.7 μl and 2.3 μl of the 1st PCR product was used as a template. The PCR amplification program for both rounds of nested PCR was performed as follows: 5 min at 95°C, 50 cycles of 30 s at 95°C, 30 s at 50°C and 55 s at 72°C, then 10 min at 72°C and cooling to 4°C. After the 2nd PCR, selected wells were tested on a 2 % agarose gel, with expected product size ~400 bp. PCR products were sequenced using Sanger sequencing by Genewiz, Leipzig, Germany.

Bulk BCR library preparation and repertoire sequencing
The library for NGS by Illumina MiSeq 2 x 300 bp paired-end sequencing was based on a 5-prime multiplex PCR method, as previously described.[40,66,67] A similar protocol was performed for both IgM and IgG library preparation but from different time points. IgM library preparation was performed from bulk PBMCs prior to immunization (week 0) while IgG library preparation was done with PBMCs 2 weeks after immunizations two and three (i.e., Boost 1 and Boost 2).

For both library preparations, the first step was RNA extraction. This step was done using the RNeasy Mini Kit (Qiagen) following manufacturer's instructions. After extraction, RNA concentration was measured with Qubit. The second step was cDNA synthesis by RT-PCR where the primers include a Unique Molecular Identifier (UMI) and an adapter tail sequence. For the IgM library, the reaction mix contained 8 μL of RNA (minimum 500 ng), 2 μL 10 mM IgM primer, 2 μL 5 mM dNTP mix (Invitrogen), and 4 μL nuclease-free water. The mix was incubated for 5 min at 65°C, followed by 5 min at 37°C, and 5 min on ice. After this, 4 μL of 5 x RT buffer, 1 μL 01 M DTT, 1 μL of RiboLock RNase inhibitor, and 1 μL SuperScript IV (All Invitrogen) were added. The mix was incubated for 10 min at 50°C, then 10 min at 80°C, and stored at 4°C until purified. The cDNA was purified using GeneJet PCR Purification Kit (Thermo Scientific) according to the manufacturer's instructions and stored at -80°C. For the IgG library, the difference was the reaction mix (IgG primer) and that the first incubation was only 5 min at 65°C and 5 min on ice. Subsequent steps were the same.

After cDNA synthesis with UMI and adapter tail addition, the multiplex PCR using the primers provided by[40,66,67] was performed. For the IgM, the reaction mix contained 5 μL of cDNA, 1 μL of 10 μM 3'Read2U primer, 2 μL 10 μM Forward Primer mix (containing Read1U sequence), 12 μL KAPA HiFi ReadyMix PCR Kit (Kapa Biosystems), and 5 μL nuclease-free water. For the PCR, the incubation was 5 min at 96°C, followed by 25 cycles of 20 s at 95°C, 20 s at 68°C, 20 s at 72°C, the last elongation for 7 min at 72°C and then stored at 4°C. Following that, the whole PCR mix was added on 1.5% agarose gel was and run for 100 mV for 30 min. The bands between 550 bp – 600 bp were excised and purified using MinElute Gel Extraction kit (Qiagen) following the manufacturer's instructions. For IgG library, the reaction mix was with 5 μL of cDNA, 1 μL of 10 μM 3'Read2U primer, 1 μL 10 μM Forward Primer mix (containing Read1U sequence), 10 μL KAPA HiFi HotStart ReadyMix PCR Kit (Kapa Biosystems), and 3 μL nuclease-free water. The PCR settings and the other steps were the same for both libraries.

Following that, the next step is the Index PCR where an identifier labels each initial library. From now on, the protocol for both IgM and IgG library preparation was the same. The reaction mix contained 5 ng of the purified PCR product, 2 μL 10mM P5_R1 Primer, 2 μL 10mM P5_R2 Primer, 25 μL KAPA HiFi HotStart ReadyMix PCR Kit (Kapa Biosystems), 21 μL nuclease-free water. The incubation was 5 min at 96°C, 30 s at 95°C, 30 s at 68°C, 30 s at 72°C, final elongation with 10 min at 72°C. After the PCR, a 1.5% agarose gel was done to confirm the absence of primer dimers. The DNA was purified using the PCR Purification Kit (Qiagen) following the manufacturers' instructions. Furthermore, a magnetic bead purification protocol using the AMPure XP Reagent for PCR Purification (Beckman Coulter). The DNA concentration was measured with the Qubit High Sensitivity dsDNA (Invitrogen) following the manufacturer's protocol. Lastly, the library pool and final sample preparation for the sequencing were performed using MiSeq Reagent Kit v3, 600 cycles (Illumina) following the manufacturer's instructions.

Analysis of BCR sequences

Sequence processing

Processing of reads and IGHV germline inference was performed using *IgDiscover* program (v. 0.15.1)[68] with default settings, except for UMI length of 21 nucleotides. The individualized IGHV germlines were generated using IgM library reads prior to vaccination with two iterations (Figures S4D and S4E), first with a starting database[33] and a second iteration adding highly divergent discovered alleles, as previously described.[67]

Germline assignments for the IgG libraries after the first and second boost were based on the inferred IGHV individualized germlines and IGHD and IGHJ alleles from Cirelli et al.[33] A biological replicate of the IgG library for the animal E17 was generated due to a low number of reads retrieved with the first biological replicate, replicates were merged and analyzed together.

Antigen-specific single-cell sorted Sanger sequences were processed and filtered using *scifer* (v. 0.9.3.) R/Bioconductor package for single-cell quality control of immunoglobulin sanger sequences (DOI: 10.18129/B9.bioc.scifer). The germline assignment of the single-cell sequences was also based on the inferred IGHV individualized germlines and IGHD and IGHJ alleles from Cirelli et al.[33] Light chain sequences from single cells were aligned to IGLV, IGLJ, IGKV, and IGKJ alleles from Cirelli et al.[33]

Clonotype assignment

Following germline assignment, the *clonotype module* from *IgDiscover* (v. 0.15.1) was used to assign clonotypes.[40] For this, we combined all the processed sequences (bulk IgG sequences from boost 1 and boost 2 as well as antigen-specific single-cell sequences) and then ran the *igdiscover clonotype* function. The combined dataset has 15 million IgG sequences with good germline assignment (approx. 0.6–1M per animal per timepoint) (Figure S5C). After clonotype assignment, clonal groups containing at least one antigen-specific single-cell sequence were selected for subsequent analysis with custom R scripts written using *R* (v. 4.2.2), *RStudio* (v. 2022.12.0+353), *ggplot2* (v. 3.4.1), *dplyr* (v. 1.1.0), *data.table* (v. 1.14.8), *scales* (v. 1.2.1), and *ggprism* (v. 1.0.4) (available at: github.com/rodrigarc/RSV-NP-repertoire). Sequences belonging to the same clonotype were defined as utilizing the same IGHV and IGHJ allele pairing, same HCDR3 length, falling within an 80% HCDR3 amino acid identity threshold, and having at least one HCDR3 junction conserved at the nucleotide level, as previously described.[40] For comparison, we also performed germline assignment with the KI macaque database (KIMDB)[67] (Figure S4M). Due to low clonotype counts specific only to PostF (~5.8% of total), individual analysis for this specificity was not computed.

Following the integration of sequencing data and the identification of antigen-specific sequences, the frequency of IGHV-IGHJ allele usage was computed and plotted. To reduce allele nomenclature complexity, allele names were collapsed to gene names. The gene usage frequency was calculated considering the total count of antigen-specific sequences at both Boost 1 and Boost 2 per animal. The arithmetic mean value per group resulting from these calculations is displayed in the heatmap (Figure 5I).

Clonotype diversity indices

After clonotype assignment, the distribution of antigen-specific clonotype sizes for each animal were used for estimating diversity indices using the R *vegan* package (v. 2.5.7) for estimating bias-corrected Chao1 species richness index.[86] Clonal sizes were sub-sampled 100 times for species richness estimation based on the lowest number of total antigen-specific sequences among individual animals per timepoint to reduce bias due to different sequencing depth. The arithmetic means of these replicates was calculated and used for plotting. The *Recon* program (v. 2.5) was used with the default settings and with the standard workflow for estimating Hill numbers,[71] the species richness index was used for plotting.

Clonotype lineage tracing

Using the processed data generated after clonotype assignment, the nucleotide sequences of interest (LOR21, LOR24, and LOR74 clonotypes) were retrieved and used for phylogenetic analysis. The sequences were aligned using the multiple sequence alignment tool MUSCLE (v 5.1)[69] with the default settings. Aligned sequences were used as input for FastTree (v 2.1.11)[70] using the generalized-time reversible model for nucleotide sequences.[87] The unmutated common ancestor (UCA) sequences used in the trees were generated by joining the assigned germline V allele and J allele before the multiple sequence alignment, leading to automatic insertion of gaps in the CDR3 region. The phylogenetic trees had their metadata merged and were re-rooted to their UCA using *treeio* (v. 1.22.0)[72] and plotted using *ggtree* (v. 3.6.2).[73]

In addition to tracing lineages by clonotype definition, the LOR24 mature sequence was also compared to all the IgG libraries from each animal. In this case, the Levenshtein distance was calculated between the LOR24 amino acid VDJ sequence and every other VDJ sequence using the *stringdist* (v. 0.9.10) R package. The resulting values were converted to identity percentages based on the LOR24 sequence length and used to plot 2D-histograms based on amino acid identity and somatic hypermutation percentages using *ggplot2* (v. 3.4.1).

Determination of inferred UCAs

The heavy chain UCAs were inferred by reverting the amino acid sequences to their assigned germline IGHV and IGHJ alleles, while retaining an identical HCDR3 to the mature sequences. The light chain UCAs were similarly inferred by reverting the amino acid sequences to their assigned germline IGKV/IGLV or IGKJ/IGLJ alleles. For the LOR21 UCA, a heavy chain sequence was retrieved in the boost 1 IgG library that had only two synonymous nucleotide mutations and an identical HCDR3 to the mature sequence.

Biolayer interferometry analyses

Accessibility profile of RSV-F antigens and assembled nanoparticles

Binding of reference antibodies to RSV-F antigens was performed and analyzed using an Octet Red 96 System (Pall FortéBio/Sartorius) at ambient temperature with shaking at 1000 rpm. The antibodies D25,[36] Palivizumab,[37] LOR33 (described here), and LOR45

(described here) were immobilized onto ProA biosensors (FortéBio) to a ~2 nm shift at 5 μg/mL in Kinetics buffer (1× HEPES-EP+ buffer (Pall FortéBio), 0.05% nonfat milk, and 0.02% sodium azide), followed by a wash using Kinetics buffer for 30 s. Association was measured for 200 s at 100 nM of DS-Cav1 antigen for DS-Cav1, DS-Cav1-I53-50A component, 20-mer, 10-mer, and bare I53-50 nanoparticle in black 96-well Greiner Bio-one microplate at 200 μL per well. Dissociation was measured by inserting the biosensors back into Kinetics buffer for 200 s. The data were baseline subtracted using the Pall FortéBio/Sartorius analysis software (version 12.0) and plotted using Prism version 9 (GraphPad Software Inc.). The greater mass (and thereby greater signal) of each bound nano-particle was considered for interpretations of measured shifts, as previously reported.[17,18]

Antigenicity profile of RSV-F antigens and nanoparticle component

Binding of reference antibodies to RSV-F antigens was performed and analyzed using an Octet Red 96 System (Pall FortéBio/Sartorius) at ambient temperature with shaking at 1000 rpm. The antibodies AM14,[61] D25,[36] and 4D7[60] were immobilized onto ProA biosensors (FortéBio) for 100 s at 10 μg/mL in Kinetics buffer, followed by a wash using Kinetics buffer for 30 s. Association was measured for 200 s at 100 nM of DS-Cav1, SC-DM, DS-Cav1-I53-50A component, or postF in black 96-well Greiner Bio-one microplate at 200 μL per well. Dissociation was measured by inserting the biosensors back into Kinetics buffer for 200 s. The data were baseline subtracted using the Pall FortéBio/Sartorius analysis software (version 12.0) and plotted using Prism version 9 (GraphPad Software Inc.).

Affinity determination of LOR Fab and IgG samples

Affinity determinations were performed and analyzed using an Octet Red 96 System (Pall FortéBio/Sartorius) at ambient temperature with shaking at 1000 rpm. The prefusion-stabilized RSV-F trimer SC-DM or the postF trimer was diluted to 5 μg/mL in Kinetics buffer and immobilized onto Anti-Penta-HIS biosensors (HIS1K; FortéBio) for 70 s, followed by a wash using Kinetics buffer for 30 s. LOR Fabs or IgGs were diluted to 300 nM or 100 nM in Kinetics buffer and serially diluted three-fold to concentrations of 1.23 nM or 0.411 nM. Reagents were applied to a black 96-well Greiner Bio-one microplate at 200 μL per well as described below. Fab and IgG association was performed by dipping the HIS1K biosensors with immobilized immunogen into diluted LOR Fab or IgG for 200 s, then dissociation was measured by inserting the biosensors back into Kinetics buffer for 200 s. The data were baseline subtracted and the plots fitted using the Pall FortéBio/Sartorius analysis software (version 12.0) assuming a 1:1 binding model. Calculated affinity constants, KD for Fabs and apparent KD for IgGs, is plotted.

Electron microscopy analyses

Negative-stain EM sample preparation (nanoparticle component antigenicity)

DS-Cav1, postF, and the DS-Cav1-I53-50A cage component were diluted to 0.08 mg/mL for negative stain. 3 μL of the diluted complexes were immediately negatively stained using Gilder Grids overlaid with a thin layer of carbon and 2% uranyl formate as previously described.[88] Fabs of the antibody 4D7[60] were generated using the Pierce Fab generation kit. The 4D7 Fab complexes with DS-Cav1, DS-Cav1-I53-50A, and postF followed a similar staining protocol, but were first allowed to associate at a starting concentration of 1 μM F monomer in 25 mM Tris (pH 7.5) 50 mM NaCl, with a 2x molar excess of Fab. The complexes were then allowed to incubate on ice for approximately 30 minutes before being diluted to 0.08 mg/mL and immediately negatively stained (to avoid concentration induced disassembly of the complex).

Negative-stain EM data collection and processing (nanoparticle component antigenicity)

Data were collected on an FEI Technai 12 Spirit 120 kV electron microscope equipped with a Gatan Ultrascan 4000 CCD camera. A total of ~150 images were collected per sample by using a random defocus range of 1.1–2.0 μm with a total exposure of 45 e−/A². Data were automatically acquired using Leginon,[74] the parameters of the contrast transfer function (CTF) were estimated using CTFFIND4,[75] and particles were picked in a reference-free manner using in cisTEM.[76] Particles were extracted after correcting for the effect of the CTF for each micrograph with cisTEM.[76] Particle stacks were exported and pre-processed in RELION/3.1.[77–79] Resulting particles were sorted by reference-free 2D classification over 25 iterations.

Negative-stain EM sample preparation (antibody epitope mapping)

Each Fab/SC-DM complex was formed at a starting concentration of either 1 μM SC-DM or RSV PostF monomer in 25 mM Tris (pH 7.5) 50 mM NaCl, with a 1.5x molar excess of Fab. Complexes were allowed to incubate on ice for approximately 1 minute before being diluted to 0.1 mg/mL for negative stain. 3 μL of the diluted complexes were immediately negatively stained (to avoid fab-induced disassembly over time) using Gilder Grids overlaid with a thin layer of carbon and 2% uranyl formate as previously described.[88]

Negative-stain EM data collection and processing (antibody epitope mapping)

Data were collected on an Talos L120C 120kV electron microscope equipped with a CETA camera. A total of ~350 images were collected per sample by using a random defocus range of 1.3–2.3 μm, with a total exposure of between 30 and 50 e−/A², with a pixel size of 2.49 Å/pixel. All data were automatically acquired using EPU (ThermoFisher Scientific). A subset of the complexes was collected using additional tilt angles spanning ranging between 5 and 45 degrees. All data processing was performed using Cryo-SPARC.[80] The parameters of the contrast transfer function (CTF) were estimated using CTFFIND4,[75] and particles were picked initially in a reference-free manner using blob picker, followed by template picking using well-defined 2D classes of intact nanoparticles. Particles were extracted after correcting for the effect of the CTF for each micrograph with a box size of 160 pixels. Extracted particles were sorted by reference-free 2D classification.

BCR transgenic B cell lines

The D25, MPE8, and LOR24_UCA BCR RAMOS cell lines were generated by lentiviral transduction of surface-IgM-negative RAMOS cells (ATCC: CRL-1596) as previously described.[89,90] In brief, Genscript synthesized and cloned the variable regions of the heavy and light chain of the respective antibodies into separate expression vectors containing fluorescent reporter genes (pLVX-ZsGreen and pLVX-mCherry, both from Clontech) and the respective consensus human IgM constant regions (expression vectors kindly shared by Adrian McDermott, VRC). Lentiviral packaging of the IgM expression vectors was achieved by co-transfection with Lipofectamine 2000 (ThermoFisher) in HEK293T cells (ATCC: CRL-3216) with the packaging plasmid psPAX2 and the vesicular stomatitis virus envelope protein G (VSV-G)-expressing plasmid pMD2.G (both from Addgene). Supernatants were harvested 3 days after transfection. Centrifugation-clarified supernatants were used for transduction of RAMOS cells with both heavy and light chains. Transduced cells were enriched by cell sorting after 5 days using a BD Aria III Fusion cell sorter. Multiple rounds of cell sorting enriched cells for stable fluorescence from both reporter proteins as well as high surface-IgM expression.

For Ca^{2+}-flux experiments, cells were stained with Fura Red (ThermoFisher) in serum-free DMEM media for 30 minutes and then washed. Stained cells were aliquoted at 1 million cells per tube in 0.3 mL media, kept at RT, and warmed at 37°C for 2 minutes immediately before use. Acquisition was performed on a LSR Fortessa flow cytometer (BD Biosciences), and baselines were recorded for 30 seconds for each sample before addition of antigens to measure BCR-specific activation for an additional 150 seconds. Mouse anti-human IgM F(ab')$_2$ (Southern Biotech) was used as a positive control that cross-links BCRs and to measure the maximal signal. The FuraRed ratio (fluorescence in BV650 / fluorescence in PerCP-Cy5.5) of bound and unbound calcium over time was used for analysis.

QUANTIFICATION AND STATISTICAL ANALYSIS

No statistical methods were used to predetermine sample size. Statistical parameters including the exact value of n, the definition of center, dispersion, and precision measures are reported in the Figures and Figure Legends. Data were judged to be statistically significant when $p < 0.05$. In Figures, adjusted p-values are reported and the statistical tests used for comparisons is specified in the respective Figure Legends. Analyses were performed in Prism version 9 (GraphPad Software Inc.) or in *R* (v. 4.2.2).